Bioresource Technology 450 (2026) 134464

Contents lists available at ScienceDirect

Bioresource Technology

journal homepage: www.elsevier.com/locate/biortech

Citrate-enabled process intensification reinforces energy and redox metabolism for sustainable bioproduction using *Corynebacterium glutamicum*

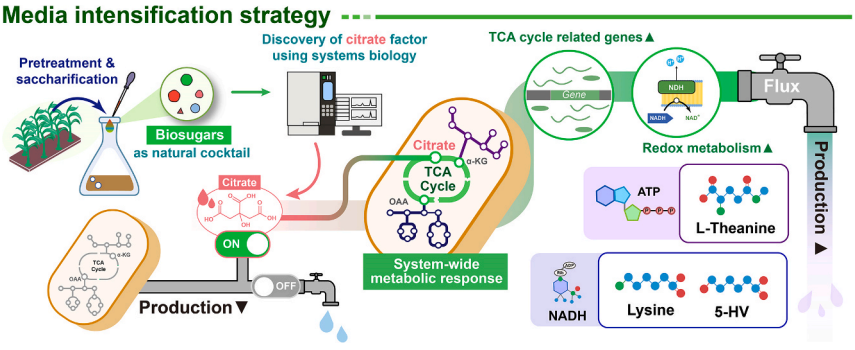
KwangYoung Park [a,1], Hoe-Suk Lee [b,1], Dong Young Lee [c,1], June-Ho Choi [d,1], Yunhee Jeong [a], SunJoo Park [a], Yunjeong Song [a], Jiyoung Park [a], Chan-Duck Jung [d], Hoyong Kim [d], Sung-Hyun Jo [e], Yun-Gon Kim [e], Yung-Hun Yang [f], See-Hyoung Park [g], Kyungmoon Park [g], Si Jae Park [h], Jungoh Ahn [i], Eun Ju Yun [c,*], Young Joo Yeon [b,*], Hee Taek Kim [a,*]

[a] *Department of Food Science and Technology, Chungnam National University, Daejeon 34134, the Republic of Korea*
[b] *Department of Biochemical Engineering, Gangneung-Wonju National University, Gangneung 25457, the Republic of Korea*
[c] *Department of Biotechnology, The Catholic University of Korea, Bucheon 14662, the Republic of Korea*
[d] *Center for Bio-based Chemistry, Korea Research Institute of Chemical Technology (KRICT), Ulsan 44429, the Republic of Korea*
[e] *Department of Chemical Engineering, Soongsil University, Seoul 06978, the Republic of Korea*
[f] *Department of Biological Engineering, College of Engineering, Konkuk University, Seoul 05029, the Republic of Korea*
[g] *Department of Biological and Chemical Engineering, Hongik University, Sejong 30016, the Republic of Korea*
[h] *Department of Chemical Engineering and Materials Science, Graduate Program in System Health Science & Engineering, Ewha Womans University, Seoul 03760, the Republic of Korea*
[i] *Biotechnology Process Engineering Center, Korea Research Institute of Bioscience and Biotechnology, Cheongju 28116, the Republic of Korea*

HIGHLIGHTS

- Biosugars served as natural test cocktails to identify bioprocess-enhancing factors.
- Citrate was a key enhancer of L-theanine biosynthesis in *C. glutamicum*.
- Citrate reinforced TCA flux, increased ATP levels, and reduced lactate overflow.
- Citrate-mediated energy boosting extended beyond ATP to NADH-dependent pathways.
- Citrate feeding enabled energy-demanding biosynthesis beyond metabolic engineering.

GRAPHICAL ABSTRACT



ARTICLE INFO

Keywords:
Corynebacterium glutamicum
L-theanine biomanufacturing
Citrate-enabled intensification

ABSTRACT

Intensification of media components can effectively improve biochemical production by reinforcing the metabolic capacity of engineered strains. Here, we present a citrate-enabled medium intensification strategy for sustainable L-theanine biomanufacturing in *Corynebacterium glutamicum*. Recombinant strains expressing

* Corresponding authors.
E-mail addresses: ejyun@catholic.ac.kr (E.J. Yun), yjyeon@gwnu.ac.kr (Y.J. Yeon), heetaek@cnu.ac.kr (H.T. Kim).
[1] These authors contributed equally to this work.

https://doi.org/10.1016/j.biortech.2026.134464
Received 22 January 2026; Received in revised form 7 March 2026; Accepted 18 March 2026
Available online 21 March 2026
0960-8524/© 2026 The Author(s). Published by Elsevier Ltd. This is an open access article under the CC BY-NC-ND license (http://creativecommons.org/licenses/by-nc-nd/4.0/).

Sweet sorghum bagasse-derived biosugar
Energy metabolism
Metabolic engineering

heterologous theanine synthases were constructed using a strain expressing L-glutamate–L-cysteine ligase from *Escherichia coli* (THE-6) to achieve high theanine production. To establish a sustainable process, renewable biosugars derived from hydrothermally pretreated sweet sorghum bagasse were used as fermentation feedstock. Cultivation with biosugar-based media significantly enhanced theanine titers compared to cultivation with analytical-grade sugars. Integrated metabolic profiling using biosugars as natural test cocktails identified citrate as a key medium-derived factor that enhanced productivity. Controlled citrate supplementation improves theanine production. Integrated metabolomic–transcriptional analyses suggest that citrate accelerates TCA cycle-driven oxidative metabolism and elevates intracellular ATP availability, thereby enhancing precursor utilization toward theanine biosynthesis. Under carbon-equivalent conditions, citrate supplementation increased theanine titers by up to approximately 1.5-fold and improved carbon yields by approximately 10–30% compared to glucose-only controls. Notably, the citrate-enabled intensification effect extended beyond ATP-intensive theanine biosynthesis to NADH-dependent pathways, including lysine, glutaric acid, and 5-hydroxyvaleric acid production, resulting in approximately 1.2- to 2.5-fold increases in product titers depending on the pathway configuration, consistent with strengthened cellular redox metabolism. Overall, the proposed biosugar-guided, integrated metabolomics–transcriptional analysis approach revealed effective media intensification factors and demonstrated that citrate supplementation can broadly strengthen cellular energy and redox metabolism. These findings support citrate-enabled medium intensification as a complementary energy- and redox-reinforcement strategy alongside conventional metabolic engineering.

1. Introduction

Accelerated climate change and resource depletion demand a shift from extraction-based manufacturing to the sustainable biomanufacturing of functional ingredients. Advances in enzyme and metabolic engineering have enabled the microbial production of functional ingredients such as 5-aminovaleric acid (Jeong et al., 2025), γ-aminobutyric acid (Son et al., 2022), and L-theanine (Mu et al., 2015) within relatively short cultivation periods using sugar-based feedstocks. Nevertheless, translation to an industrial scale is limited by persistent technical challenges, including strain performance and process robustness. Accordingly, next-generation biomanufacturing is increasingly integrating strain engineering with process-level optimization, such as pH control (Regueira-Marcos et al., 2023), organic acid supplementation (Wehrs et al., 2019), micronutrient availability (van Dijk et al., 2020), and redox balance (Akiyama and Osanai, 2024). Therefore, the identification of effective bioprocess-enhancing factors that complement genetic and metabolic engineering is essential for advancing precise biomanufacturing. In particular, organic acid supplementation, including succinate, acetate, or citrate, has been widely applied to improve microbial fermentation performance, primarily by serving as auxiliary carbon sources or anaplerotic precursors to replenish TCA cycle intermediates (Yang et al., 2016; Chang et al., 2020; Schulz et al., 2023; Chen et al., 2018). In most cases, the resulting improvements in productivity have been interpreted from a precursor-feeding or co-substrate utilization perspective, emphasizing redistribution of carbon flux toward target products. However, systematic investigation into how such supplementation influences global cellular energetics and intracellular redox balance under controlled conditions remains limited. Similarly, productivity enhancements observed in lignocellulosic hydrolysate–based (biosugar) media have often been attributed to medium complexity or nutrient diversity, while the specific productivity-enhancing components and their mechanistic roles have remained insufficiently defined (Han et al., 2019).

Bioproduction of value-added compounds often relies on metabolic pathways that demand substantial cellular energy and reducing power, primarily in the form of ATP and NADH/NADPH. These cofactors, which are indispensable for driving biosynthetic reactions, compete for essential growth and maintenance processes. Consequently, even with optimized enzymatic reactions and carbon flux redistribution, product titers plateau owing to imbalanced intracellular energy and redox states. This has been observed for L-theanine, a non-proteinogenic amino acid naturally present in tea (*Camellia sinensis*) leaves, which is responsible for its umami flavor and established physiological effects such as stress relief and cognitive enhancement (Li et al., 2022). Microbial biosynthesis of L-theanine requires one molecule of ATP per γ-glutamyl bond formation catalyzed by γ-glutamylmethylamide synthetase (GMAS), directly linking product formation to intracellular ATP availability (Wang et al., 2021). Recent metabolic engineering strategies to enhance L-theanine production include heterologous GMAS expression, competing pathways elimination, precursor supply reinforcement, and ATP regeneration approaches. Early shake-flask systems achieved gram*per*-liter titers (Wang et al., 2021), whereas subsequent protein engineering and pathway optimization in fed-batch processes enabled production levels exceeding 40 g/L under optimized conditions (Yang et al., 2024). To alleviate ATP limitation, polyphosphate kinase 2 has been introduced to regenerate ATP from polyphosphate, resulting in 1.5- to 2.0-fold titer improvements (Cho et al., 2024). Similarly, a de novo glucose-based E. coli pathway integrating precursor enhancement, TCA rewiring, and ATP regeneration achieved 22.6 g/L of L-theanine with a 41.7% yield (Zhou et al., 2025). However, such cofactor engineering strategies may impose additional metabolic burden associated with polyphosphate turnover, potentially affecting long-term stability and scalability. These considerations highlight the need for alternative strategies to reinforce cellular energy and redox metabolism through less invasive interventions.

Media intensification strategies, including modification of cultivation medium composition or metabolomics-guided supplementation, represent valuable complements to metabolic engineering for improving product titers and yields (Wan et al., 2023). Previous strategies involved phosphate supplementation in Escherichia coli-based threonine biosynthesis (Yang et al., 2022); cysteine supplementation to relieve CoA imbalance and increase 1-butanol titers (Ohtake et al., 2017); succinate and amino acid supplementation combined with carbon-to-nitrogen ratio optimization, which increased pyridoxine (the major commercial form of vitamin B6) titers 1.71-fold (Tian et al., 2024); and vitamin supplementation coupled with pantothenate kinase overexpression in Yarrowia lipolytica, which enhanced β-farnesene production 1.49-fold (Liu et al., 2023). However, systematic efforts targeting the central energy metabolism, particularly ATP generation, are lacking.

Biomass-derived hydrolysates (biosugars), which are valuable alternative carbon sources, contain complex pools of medium-derived components that harbor bioprocess-enhancing factors and can be exploited as natural test cocktails for media intensification. For example, engineered *Corynebacterium glutamicum* produces up to 98.6 g/L succinate from corn stover hydrolysate, which is 1.06-fold higher than that obtained from glucose–xylose mixtures (Mao et al., 2018). Sasaki et al. (2019) achieved isopentenol production from sorghum hydrolysate despite residual ionic liquids, whereas Zhong et al. (2025) reported L-homoserine yields of 93.1 g/L from lignocellulose-derived hydrolysate, representing a 1.37-fold increase from that obtained from a glucose medium using strains capable of co-utilizing multiple sugars. However,

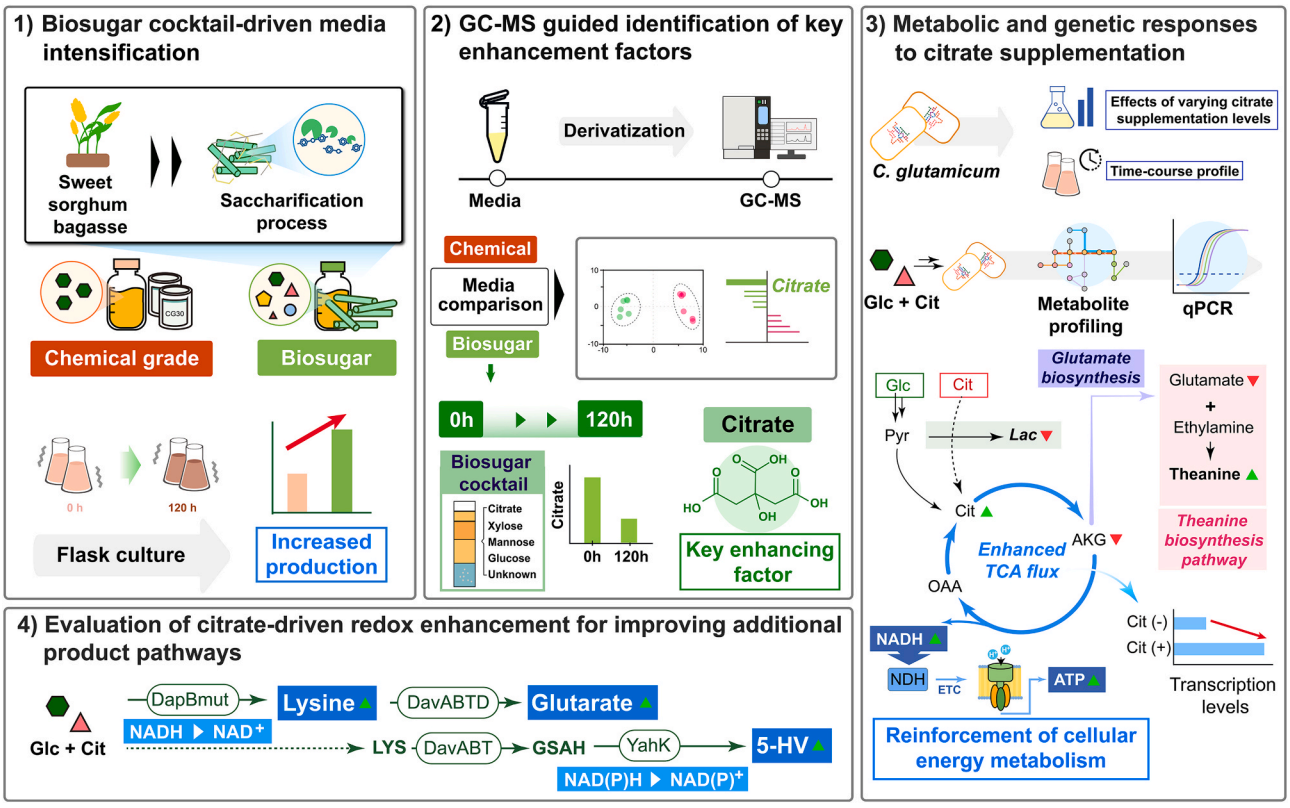


Fig. 1. Overall scheme of a platform for discovering media intensification factors. The strategy integrates comparative media analysis with systems-level biological tools to identify medium components that enhance intracellular metabolic performance and bioproduction. GC–MS, gas chromatography–mass spectrometry; qPCR, quantitative polymerase chain reaction; TCA, tricarboxylic acid; OAA, oxaloacetic acid.

strategies for identifying and leveraging medium-derived components to reinforce cellular energy and redox metabolism in a generalized manner require further investigation.

As a proof-of-concept, we propose biosugars as natural test cocktails to uncover medium-derived productivity enhancers and demonstrate a citrate-enabled process intensification strategy for sustainable L-theanine biomanufacturing in *C. glutamicum* (Fig. 1). Rather than treating biomass-derived hydrolysates merely as alternative carbon sources, we conceptualized them as structured complexity platforms for identifying medium-level metabolic reinforcement factors. By leveraging their compositional diversity as natural test cocktails, we aimed to systematically uncover productivity-enhancing components that could be subsequently validated at the systems level. In this study, we combined docking-based enzyme screening and biosugar component profiling to identify citrate as a key productivity-enhancing factor. Integrated metabolomics, ATP quantification, and transcriptional profiling revealed that citrate reinforces cellular energy metabolism by coordinating ATP generation and redox balance, thereby enhancing the efficiency of precursor use. We further validated the generality of this approach by applying citrate supplementation to NADH-dependent biosynthetic pathways including lysine, glutarate, and 5-hydroxyvaleric acid (5-HV) production. Accordingly, this study introduces a medium-level, energy-focused strategy for precision biomanufacturing that complements genetic and metabolic engineering for the sustainable production of high-value functional ingredients. Beyond basic TCA intermediate supplementation, citrate-enabled intensification reinforces oxidative metabolism and cofactor regeneration at the systems level, offering insight into how medium-derived factors can enhance biosynthetic efficiency.

2. Materials and methods

2.1. Strains and plasmids

The strains and plasmids used in this study are listed in Table 1. *E. coli* DH5α (Invitrogen™, Thermo Fisher Scientific, Waltham, MA, USA) was used for gene cloning and plasmid maintenance. The *C. glutamicum* KCTC1852 strain was purchased from the Korean Collection for Type Cultures (KCTC, Republic of Korea) and engineered to produce theanine. All DNA manipulations were conducted following standard procedures. A C1000 Thermal Cycler (Bio-Rad, Hercules, CA, USA) was used for the PCRs. The primers used were synthesized by Cosmo Genetech (Seoul, Republic of Korea). The *gmas* genes from *Methylovorus mays* and *Rhodovulum* sp. 12E13, along with the *gshA* (i.e., *Ecgcs*) gene from *E. coli*, were PCR-amplified, digested with *Bam*HI/*Spe*I, and ligated into the corresponding sites of pCES208H30 or pCES208H36. The *xylAB* gene cluster from *E. coli* was amplified, digested with *Eco*RI/*Kpn*I, and ligated into the corresponding sites of pBL712H30 for co-expression of xylose isomerase and xylose kinase (see supplementary materials). One of the pCES208 plasmids, containing either *gmas* or *Ecgcs* genes, was co-transformed with pBL712H30XylAB in *C. glutamicum* to engineer six putative theanine-producing recombinant strains (THE-1 to THE-6).

2.2. Molecular modeling of theanine synthases

The crystal structures of EcGCS and RhGMAS (L-glutamate–L-cysteine ligase from *Escherichia coli*; PDB ID: 2D33 and GMAS from *Rhodovulum* sp. 12E13; PDB ID: 7CQN, respectively) were obtained from

the Protein Data Bank. The structures of other GCSs and GMASs were constructed using the AlphaFold server. All protein structures were processed with the Protein Preparation Wizard in Maestro to assign bond orders, add hydrogen atoms, optimize protonation states at physiological pH (7.0 ± 0.2) using Epik, remove water molecules beyond 5 Å from heteroatoms, and perform restrained energy minimization with the OPLS4 force field. The ligands were prepared with LigPrep (Maestro v14.2.118), generating relevant tautomers and ionization states at pH 7.0 ± 0.5, followed by minimization with the OPLS4 force field.

Docking grids were generated using Glide (Maestro v14.2.118) at the catalytic regions defined by known substrate-binding residues centered on the ATP-binding pockets in EcGCS and MmGMAS. A cubic grid of 15 × 15 × 15 Å was used, with van der Waals scaling set to 1.0 and a partial charge cutoff of 0.25. Docking simulations were performed in Glide using standard precision mode, with a maximum of 20 poses retained per ligand, and post-docking minimization was applied. The nonpolar atoms were scaled with a van der Waals factor of 0.80. To validate the docking protocol, native ligands or ATP analogs were docked whenever available. The predicted poses were compared with the crystallographic binding modes. Docking results were scored using GlideScore, and the top-ranked conformations were further examined for hydrogen bonding, electrostatic, and stacking interactions within Maestro using the Ligand Interaction Diagram tool. Figures of docking poses were generated in PyMOL.

2.3. Culture conditions

E. coli was grown in Luria–Bertani (LB) medium containing 10 g/L tryptone, 5 g/L yeast extract, and 5 g/L NaCl at 37 °C and 200 rpm. Recombinant *C. glutamicum* KCTC1852 strains used for theanine production were grown in RG medium. Shake-flask cultures were performed in 250 mL baffled flasks containing 20 mL of CG50 medium. For experiments evaluating the effects of biomass-derived carbon sources and citrate supplementation, CG30 and CG39 media were used. The compositions of RG and CG media are listed in supplementary materials. Glucose was sterilized separately by autoclaving before addition to the medium to prevent the Maillard reaction. Next, 15 g/L $CaCO_3$ was added to the culture medium to minimize pH fluctuations during cultivation. *E. coli* strains were cultivated with 30 μg/mL kanamycin. *C. glutamicum* strains were cultivated with either 20 μg/mL kanamycin or 200 μg/mL spectinomycin, depending on the selection marker. Cell growth was monitored by measuring absorbance at 600 nm (OD_{600}) using a UV-1900i spectrophotometer (Shimadzu, Tokyo, Japan). For the comparative screening of the three heterologous theanine synthases, RhGMAS, MmGMAS, and EcGCS, each enzyme was individually expressed in *C. glutamicum*. The resulting strains were evaluated for theanine production at a fixed ethylamine concentration of 200 mM. Ethylamine was added at the beginning of cultivation as the amine donor required for L-theanine biosynthesis. Its concentration was optimized based on preliminary dose–response experiments to ensure efficient production. The effects of ethylamine and citrate concentrations on theanine production were examined over ranges of 25–400 mM and 0–600 mM, respectively. To compare theanine production efficiency under different ethylamine, glucose, and citrate supplementation conditions, carbon- and substrate-normalized yields were calculated according to Eqs. (1) and (2), respectively:

$$Y_{\mathrm{The}/(\mathrm{EtA+Glc})}(\mathrm{mM/mM}) = \text{the final theanine concentration}(\mathrm{mM}) \text{ divided by the total molar amountof ethylamine and glucose supplied } (\mathrm{mM}) \quad (1)$$

$$Y_{\mathrm{The}/(\mathrm{EtA+Glc+Cit})}(\mathrm{mM/mM}) = \text{the final theanine concentration } (\mathrm{mM}) \text{ divided by the total molar amountof ethylamine, glucose, and citrate supplied } (\mathrm{mM}) \quad (2)$$

2.4. Quantitative polymerase chain reaction

RNA was extracted from *C. glutamicum* KCTC1852 strains using the TRIzol protocol. Chloroform was added to separate RNA from proteins and DNA by generating an aqueous phase. The extracted RNA was then used to synthesize cDNA with the iScript™ RT Supermix cDNA Synthesis Kit (Bio-Rad). Quantitative polymerase chain reaction (qPCR) was performed using the CFX Connect Real-Time PCR Detection System (Bio-Rad, Hercules, CA, USA). The reactions were performed with SsoAdvanced Universal SYBR Green Supermix (Bio-Rad, Hercules, CA, USA), 0.2 μM primers, and the appropriate cDNA template. The primer sequences used for qPCR are listed in supplementary materials. All reactions were conducted in triplicate. Gene expression levels were analyzed using the comparative Ct method and the results were normalized to the expression levels of the reference gene 16S rRNA.

2.5. Extraction and use of biomass-derived carbon sources

Cellic CTec3 cellulase was obtained from Novozymes (Bagsværd, Denmark). According to the Laboratory Analytical Procedures (LAP-006) developed by the National Renewable Energy Laboratory and bicinchoninic acid assay results, the filter paper activity (FPU) and total protein concentration of cellulase were 185.0 FPU/mL and 342.6 g/L, respectively. Sweet sorghum bagasse (SSB) obtained from Good Farmer Brewing Company (Yecheon, Korea) was subjected to high-pressure steam treatment at 200 °C for 10 min. This pretreatment disrupted the lignin matrix, dissolved hemicellulose, and partially hydrolyzed cellulose, thereby releasing xylooligosaccharides. The SSB was then saccharified using Cellic CTec3 at 50 °C for 72 h at 150 rpm, yielding glucose and xylose as primary carbon sources. The resulting SSB-derived carbon sources were used for theanine synthesis with ethylamine supplementation in *C. glutamicum* strains THE-4 and THE-6. The CG30 medium was prepared by replacing glucose in the CG50 medium with SSB-derived carbon sources. All other components of the CG50 medium were kept identical to ensure consistent experimental conditions.

2.6. High-performance liquid chromatography analysis

Glucose concentration was measured using high-performance liquid chromatography (Shimadzu, Kyoto, Japan). The system was equipped with a refractive index detector (RID) and an Aminex HPX-87H column (300 × 7.8 mm, Bio-Rad, Hercules, CA, USA). Elution was performed

Table 1
Strains and plasmids used in this study.

Strains and plasmids	Characteristics	Reference or source
Strains		
E. coli DH5α	*E. coli* K-12; F^-, Φ80d*lacZ*ΔM15, Δ(*lacZYA-argF*)U169, *deoR*, *recA1*, *endA1*, *hsdR17*(r_K^- m_K^+), *phoA*, *supE*44, λ^-, *thi*-1	Invitrogen
C. glutamicum KCTC 1852	L-glutamate producer	KCTC
C. glutamicum PKC	An expired industrial L-lysine-producing strain	(Sohn et al., 2022)
C. glutamicum THE-1	*C. glutamicum* KCTC 1852 with pCES208H30Rhgmas and pBL712H30XylAB	This study
THE-2	*C. glutamicum* KCTC 1852 with pCES208H36Rhgmas and pBL712H30XylAB	This study
THE-3	*C. glutamicum* KCTC 1852 with pCES208H30Mmgmas and pBL712H30XylAB	This study
THE-4	*C. glutamicum* KCTC 1852 with pCES208H36Mmgmas and pBL712H30XylAB	This study
THE-5	*C. glutamicum* KCTC 1852 with pCES208H30Ecgcs and pBL712H30XylAB	This study
THE-6	*C. glutamicum* KCTC 1852 with pCES208H36Ecgcs and pBL712H30XylAB	This study
LYS	*C. glutamicum* PKC with pBL712H30DapB$_{mut}$	This study
HV	*C. glutamicum* PKC with pCES208H30DavB$_{His}$A and pBL712H30YahK	(Sohn et al., 2021)
GTA	*C. glutamicum* PKC with pCES208H30DavB$_{His}$A and pBL712H30DavTDDapB$_{mut}$	(Sohn et al., 2022)
Plasmids		
pCES208H30Rhgmas	pCES208 derivative; P_{H30} promoter, *R.* sp. 12E13 *gmaS* gene, Km^R	This study
pCES208H30Mmgmas	pCES208 derivative; P_{H30} promoter, *M. mays gmaS* gene, Km^R	This study
pCES208H30Ecgcs	pCES208 derivative; P_{H30} promoter, *E. coli gshA* gene, Km^R	This study
pCES208H36Rhgmas	pCES208 derivative; P_{H36} promoter, *R.* sp. 12E13 *gmaS* gene, Km^R	This study
pCES208H36Mmgmas	pCES208 derivative; P_{H36} promoter, *M. mays gmaS* gene, Km^R	This study
pCES208H36Ecgcs	pCES208 derivative; P_{H36} promoter, *E. coli gshA* gene, Km^R	This study
pBL712H30XylAB	pBL712 derivative; P_{H30} promoter, *E. coli xylA* and *xylB* genes, Sp^R	This study
pBL712H30DapB$_{mut}$	pBL712 derivative; P_{H30} promoter, *E. coli* mutant *dapB* (C115G, G116C) gene, Sp^R	This study
pBL712H30YahK	pBL712 derivative; P_{H30} promoter, *E. coli yahK* gene, Sp^R	(Sohn et al., 2021)
pCES208H30DavB$_{His}$A	pCES208 derivative; P_{H30} promoter, *P. putida* KT 2440 *davB$_{His}$A* genes, Km^R	(Sohn et al., 2022)
pCES208H30DavTDDapB$_{mut}$	pCES208 derivative; P_{H30} promoter, *P. putida* KT 2440 *davTD* genes and *E. coli* mutant *dapB*(C115G, G116C) gene, Km^R	(Sohn et al., 2022)

Km: kanamycin; Sp: spectinomycin

with 5 mM H_2SO_4 at a flow rate of 0.8 mL/min at 50 °C. Glutamate, ethylamine, and theanine concentrations were analyzed by HPLC (high-performance liquid chromatography; Agilent Technologies, Santa Clara, CA, USA) equipped with a UV detector and a CAPCELL PAK C18 UG120 s5 column (250 × 4.6 mm, 5 μm, Osaka Soda, Tokyo, Japan) according to the DEEMM method. Elution was performed using mobile phases A (acetonitrile) and B (25 mM sodium acetate buffer, pH 4.8). Samples were analyzed at 284 nm using the following gradient program: 0–2 min, 20–25% A; 2–32 min, 25–60% A; and 32–37 min, 60–20% A.

2.7. Gas chromatography–mass spectrometry-based metabolomic analysis

2.7.1. Sample preparation for intracellular metabolites

Culture aliquots corresponding to OD_{600}·mL = 1 were harvested at designated time points (Shimadzu UV-1900I, Serial No. A125360, Kyoto, Japan). Intracellular metabolites were quenched by adding five volumes of precooled (−80 °C) 100% methanol (Sigma-Aldrich, CAS 67–56-1, St. Louis, MO, USA), followed by centrifugation at 16,000 × *g* for 3 min at 4 °C (Hanil Science Inc., Gimpo, Republic of Korea; M15R). The supernatant was discarded, and the pellets were stored at −80 °C.

For extraction, the pellets were thawed on ice and resuspended with 100 μL acid-washed glass beads (Sigma-Aldrich, G1145-10G, St. Louis, MO, USA) and 1.0 mL of 50% acetonitrile (Duksan Pure Chemicals Co., Ltd., Ansan, Republic of Korea; CAS No. 75–05-8). Cells were disrupted by vortexing for 3 min, followed by centrifugation at 16,100 × g for 3 min at 4 °C. Finally, 0.8 mL of the supernatant was transferred to a new tube and dried using a SpeedVac (Digital Precision Cold Trap Bath, model WCT-80; LaboGene ApS, Allerød, Denmark; ScanSpeed MaxiVac Beta).

2.7.2. Sample preparation for extracellular metabolites and control medium

For the extracellular metabolite analysis, the culture broth was centrifuged at 16,000 × *g* for 1 min at 4 °C (M15R). Twenty microliters of the supernatant were transferred into a fresh tube and dried using a SpeedVac system. For a background control, 20 μL of freshly prepared medium, that is, biosugar-based or chemically defined broth, was collected and dried under identical conditions using SpeedVac.

2.7.3. Chemical derivatization

Dried extracts were derivatized by adding 10 μL of 40 mg/mL methoxyamine hydrochloride in pyridine (Sigma-Aldrich, St. Louis, MO, USA). This was followed by vortexing for 10 s and centrifugation at 2,234 × *g* for 10 s. The mixture was incubated at 30 °C for 90 min at 1,000 rpm. Then, 45 μL of *N*-methyl-*N*-(trimethylsilyl) trifluoroacetamide (MSTFA; Sigma-Aldrich, CAS 24589–78-4, St. Louis, MO, USA) was added, vortexed for 10 s, centrifuged briefly, and incubated at 37 °C for 30 min at 1,000 rpm. Finally, 30 μL of the supernatant was collected for gas chromatography–mass spectrometry (GC–MS) analysis.

2.7.4. GC–MS analysis and data processing

Derivatized samples were analyzed using a GC–MS system (GC-2030/MS QP2020, Shimadzu GCMS-QP Series, Kyoto, Japan) equipped with an SH-I-5Sil MS capillary column (30 m × 0.25 mm, 0.25 μm film thickness) and helium as the carrier gas. One microliter of each sample was injected in split mode (split ratio, 5:1). The oven temperature was initially held at 50 °C for 1 min, then increased to 280 °C at a rate of 15 °C min^{-1} and held at 280 °C for 10 min. Mass spectra were acquired in electron ionization mode over an *m/z* range of 50–500. The ion source and interface temperature were set to 250 and 280 °C, respectively. Raw GC–MS data were processed using AMDIS for peak deconvolution (Stein, 1999). Peaks were aligned and annotated against the Golm Metabolome Database (Kopka et al., 2005) using SpectConnect (http://spectconnect.mit.edu) (Styczynski et al., 2007), and the intensities were represented as base peak heights. Data were normalized to *z*-scores (mean = 0, SD = 1) before statistical analysis.

2.8. Liquid chromatography-tandem mass spectrometry-based quantification of intracellular adenylate and NAD(H) pools

At designated time points, culture aliquots corresponding to OD_{600}·mL = 1 were harvested. Intracellular metabolites were quenched by adding two volumes of precooled (−30 °C) 40% (v/v) methanol (Sigma-Aldrich, CAS 67–56-1, St. Louis, MO, USA), followed by centrifugation at 5000 rpm for 5 min at −4 °C (Hanil Science Co., M15R). The

supernatant was discarded, and the pellets were washed with 1 mL of precooled (4 °C) 0.8% (w/w) NaCl. The pellets were resuspended in 3 mL of precooled (−80 °C) 80% (v/v) methanol spiked with L-[13C9, 15 N]phenylalanine (Sigma-Aldrich, MO, USA) at 0.1 μg/mL as an internal standard and incubated at −80 °C for 3 h. After centrifugation (5000 rpm, −4 °C, 10 min), the supernatant was collected. A second extraction was performed in the same manner for 1 h and the supernatants were pooled. To remove macromolecules and obtain the low-molecular-weight metabolite fraction, the pooled extracts were sequentially passed through 10 kDa and 3 kDa centrifugal filters (MWCO; Amicon® Ultra centrifugal filters, Sigma-Aldrich, St. Louis, MO, USA) according to the manufacturer's instructions, and the flow-through was collected after each filtration step. The final flow-through samples containing the extracted metabolites were dried using a centrifugal vacuum concentrator (Modulspin 40, Hanil Science Industrial, Korea) and stored at −80 °C until analysis.

The dried intracellular metabolite samples were dissolved in solvent A (water/acetonitrile (95:5, v/v) with 20 mM ammonium acetate and 20 mM ammonium hydroxide), and subjected to LC–MS/MS analysis. LC–MS/MS was performed using a 1260 Infinity Binary LC system coupled to a 6420 Triple Quadrupole MS (Agilent Technologies, CA, USA). The prepared metabolite sample (10 μL) was injected into the XBridge® Amide column (4.6 × 250 mm, particle size 3.5 μm, Waters, MA, USA). Solvent B was 100% acetonitrile. The LC gradient was: 0 min, 85% B; 5 min, 42% B; 16 min, 0% B; 24 min, 0% B; 25 min, 85% B; 32 min, 85% B. The flow rate was 0.4 mL/min. The capillary temperature was 300 °C. The electrospray ionization voltage was 4 kV. Quantification of each metabolite was performed using metabolite-specific multiple reaction monitoring (MRM) transitions. MS peak areas were extracted using Agilent MassHunter Qualitative Analysis software (version B.07.00) and normalized to the peak area of the internal standard.

Intracellular ATP, AMP, ADP, NADH, and NAD^+ amounts were quantified by LC–MS/MS and are reported as nmol per unit OD_{600} (nmol/OD_{600}).

2.9. Statistical analysis

Hierarchical cluster analysis (HCA) was performed in R (v4.4.1) using the pheatmap package (v1.0.12). Orthogonal partial least squares discriminant analysis (OPLS-DA), partial least squares discriminant analysis (PLS-DA), and metabolite set enrichment analysis (MSEA) were performed using MetaboAnalyst 6.0 (https://www.metaboanalyst.ca/; accessed December 3, 2025). For OPLS-DA, model performance was summarized using R^2X, R^2Y, and Q^2 values (Kim et al., 2017). For PLS-DA, the model performance was evaluated using cross-validation with R^2 and Q^2 values (Stanciugelu et al., 2024), which indicate the explained variance and cross-validated predictive ability, respectively.

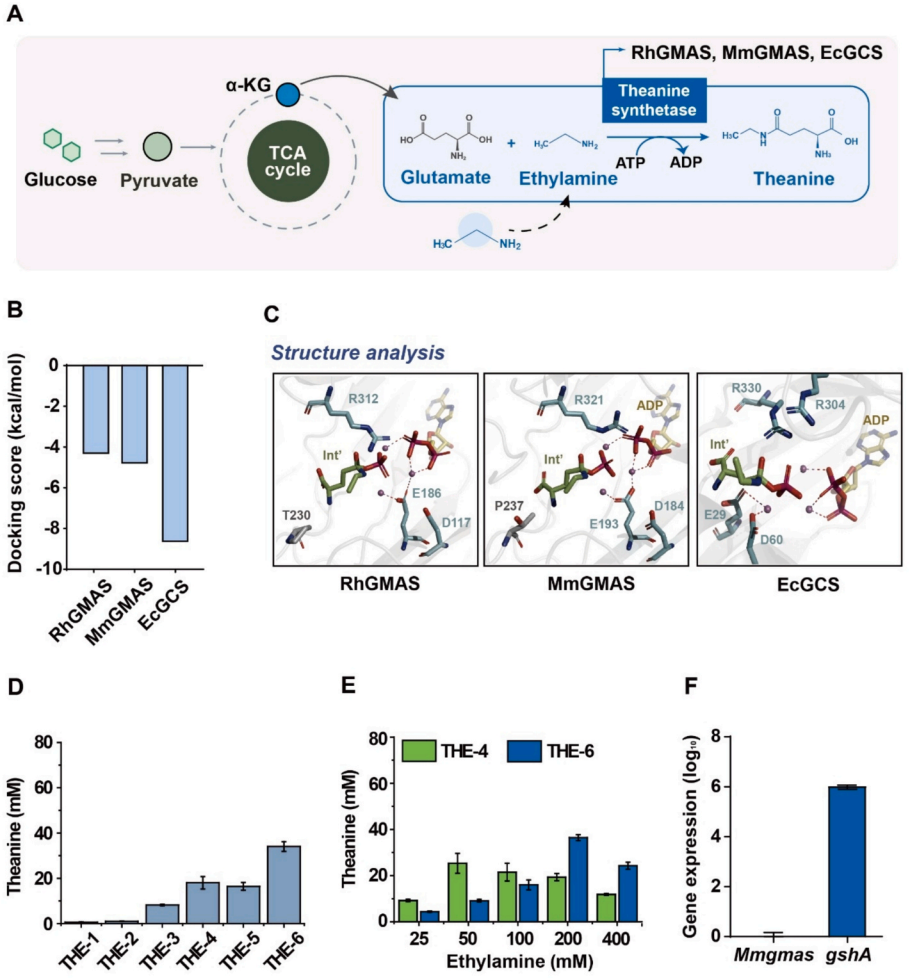


Fig. 2. Screening and validation of theanine synthetase candidates. **(A)** ATP-dependent theanine synthetase catalyzing ligation of glutamate and ethylamine. **(B)** Docking scores of RhGMAS, MmGMAS, and EcGCS with the modeled L-theanine intermediate. **(C)** Structural models showing ADP (yellow), Mg^{2+} (purple), intermediate (green), and key catalytic residues (cyan). **(D)** Theanine production by engineered strains THE-1 to THE-6. **(E)** Effect of ethylamine supplementation on theanine production. **(F)** Relative expression of the theanine synthetase gene in THE-4 and THE-6 measured by qRT-PCR (log_{10} scale). Data represent mean ± SD (n = 3). qRT-PCR, quantitative reverse transcription polymerase chain reaction; TCA, tricarboxylic acid.

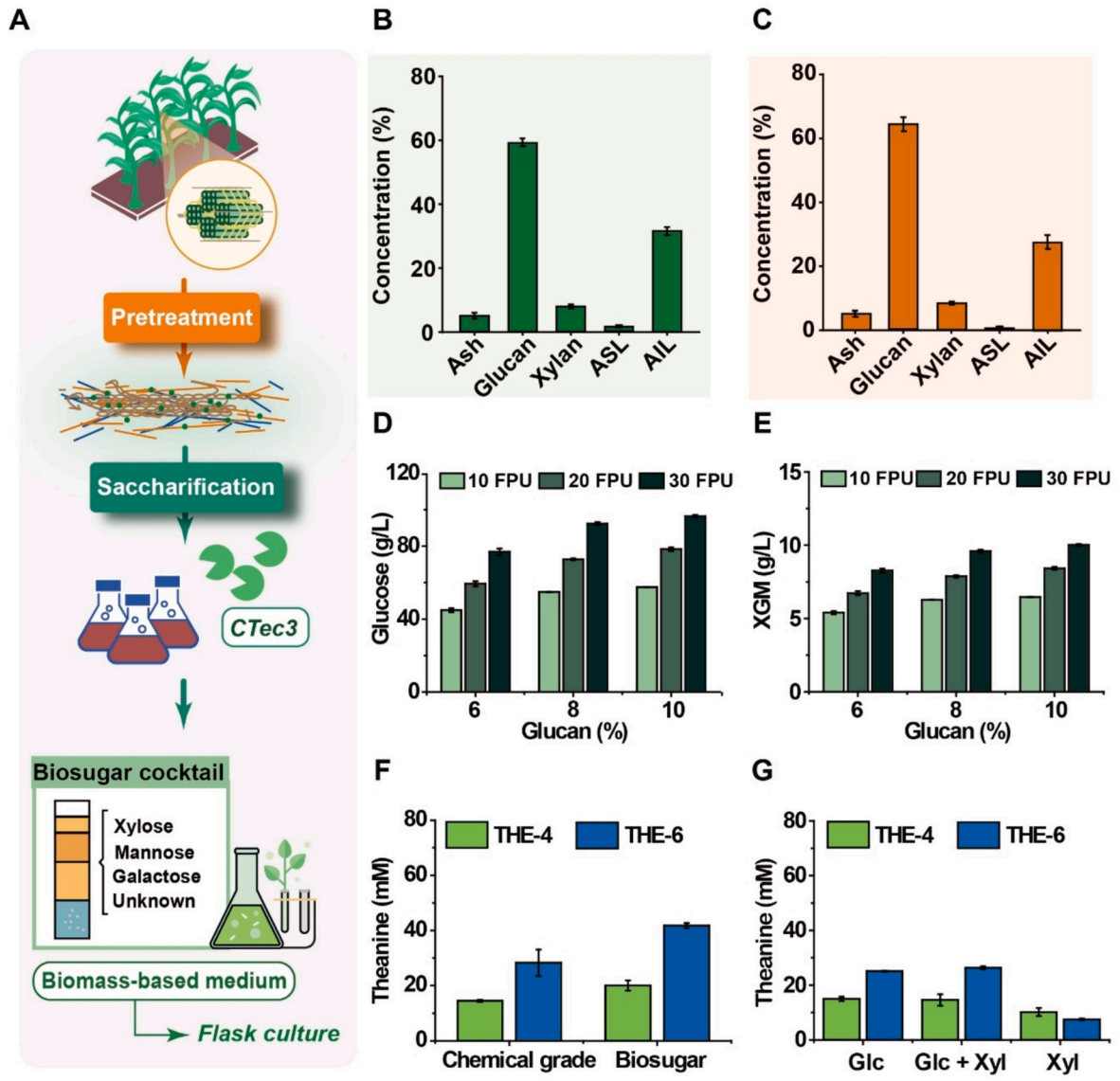


Fig. 3. Biosugar production from sweet sorghum bagasse and its application as a fermentation medium. **(A)** Process flow diagram for biosugar production via pretreatment and saccharification. **(B, C)** Composition of SSB after hydrothermal pretreatment with or without physical refining. **(D, E)** Effects of glucan loading and cellulase dosage on saccharification, shown as glucose and XGM concentrations. **(F)** Comparison of theanine production using chemical-grade and biosugar-derived carbon sources. (G) Theanine production from glucose and/or xylose. Data represent mean ± SD ($n = 3$). SSB, sweet sorghum bagasse; XGM, xylose, galactose, and mannose; ASL, acid-soluble lignin; AIL, acid-insoluble lignin; FPU, filter paper unit.

Permutation testing ($n = 1{,}000$) was conducted to assess the statistical significance of the supervised models. The variable importance in projection (VIP) scores of the first principal component were calculated. MSEA was performed using the quantitative enrichment analysis (QEA) algorithm, based on the KEGG human metabolic pathways library.

One-way analysis of variance (ANOVA) was applied, followed by Benjamini–Hochberg false discovery rate (FDR) correction for multiple testing in R. For targeted metabolite analysis, such as extracellular theanine, ANOVA was conducted without FDR correction because multiple-testing correction was unnecessary for single-metabolite analysis. Pairwise comparisons were evaluated using Tukey's honest significant difference post hoc test. Boxplots and significance levels were visualized using *ggpubr* (v0.6.0) and *ggplot2* (v3.5.2). Unless otherwise stated, all experiments were performed using at least three independent biological replicates. The number of biological replicates (n) used for each statistical analysis is reported in the corresponding figure legends.

3. Results and discussion

3.1. Development of a theanine-producing recombinant C. glutamicum strain engineered with a novel theanine synthase

Current microbial platforms for theanine production are largely based on MmGMAS (Cho et al., 2024), which catalyzes ATP-dependent condensation of glutamate and ethylamine (Fig. 2a). To identify alternative theanine synthases as candidates for experimental evaluation, docking-guided prioritization of 16 GMASs and GCSs was performed using a modeled tetrahedral intermediate. Here, γ-glutamyl phosphate was covalently linked to ethylamine to represent the modeled intermediate. Because docking provides an approximate, qualitative estimate of binding complementarity, it was used primarily to narrow candidates for subsequent *in vivo* evaluation. Based on the docking simulation results, two additional candidate enzymes, RhGMAS and EcGCS, were

prioritized, exhibiting docking scores of − 4.40 kcal/mol and − 8.72 kcal/mol, respectively, while MmGMAS scored − 4.87 kcal/mol under the same scoring function (Fig. 2b) (Xiao et al., 2023). These scores were used for relative prioritization within the screening workflow. Accordingly, RhGMAS and EcGCS were carried forward for experimental evaluation alongside MmGMAS. Structural models of the docked intermediate are provided to visualize the active-site context (Fig. 2c). Although RhGMAS and MmGMAS share similar overall folds, they differ at a position near the substrate glutamate backbone amino group (Thr230 in RhGMAS versus Pro237 in MmGMAS) (Wang et al., 2021; Yamamoto et al., 2008). EcGCS adopts a distinct fold and active-site configuration from GMAS enzymes; nevertheless, docking suggested that the modeled intermediate could be accommodated in all three enzymes in poses compatible with ADP binding, providing a structural basis for subsequent experimental testing. These results provide a rationale for prioritizing candidate theanine synthases through docking analysis. The selected enzymes were introduced into *C. glutamicum,* which was chosen based on its established industrial application in amino acid production and its high intrinsic glutamate-producing capacity. As a host chassis, *C. glutamicum* KCTC1852, a well-known glutamate-overproducing strain, was used to facilitate theanine overproduction. To construct the recombinant strains, each theanine synthase gene (*Mmgmas*, *Rhgmas*, or *Ecgcs*) was individually expressed under either the H30 or H36 promoter in the pCES208 vector backbone and introduced into *C. glutamicum* KCTC 1852. The xylose utilization module (*xylA* and *xylB*) was co-expressed from the pBL712 vector (pBL712H30XylAB). Accordingly, six recombinant strains (THE-1 to THE-6) were generated, each harboring a distinct combination of synthase gene and promoter, as is summarized in Table 1. In CG50 medium supplemented with 200 mM ethylamine, strain THE-6 expressing EcGCS under the H36 promoter achieved the highest theanine titer of 34.04 mM (5.93 g/L). In contrast, under the same conditions, strain THE-4, expressing *Mmgmas* under the same promoter produced 18.06 mM (3.15 g/L) (Fig. 2d). To determine the optimal concentration of ethylamine for theanine production, strains THE-4 and THE-6 were cultivated with varying ethylamine concentration levels (25–400 mM). THE-4 achieved its highest titer at 50 mM ethylamine, reaching 25.32 mM (4.40 g/L) with a yield of 0.077 mol/mol. In contrast, THE-6 reached a maximum titer at 200 mM ethylamine, producing 36.45 mM (6.35 g/L) theanine with a comparable yield of 0.076 mol/mol. Accordingly, 50 and 200 mM ethylamine were selected as the optimal concentrations for THE-4 and THE-6, respectively. All subsequent experiments were conducted under these conditions (Fig. 2e). The qPCR analysis indicated differences in the transcriptional levels of *Ecgcs* and *Mmgmas*, which may have partially contributed to the observed variation in theanine production (Fig. 2f). The superior activity of EcGCS highlights its potential as a promising candidate theanine synthase for further metabolic optimization and process development.

3.2. Theanine biosynthesis by recombinant C. glutamicum using biosugars from SSB as a pool of bioprocess-enhancing factors

Lignocellulosic biomass-derived hydrolysates (biosugars) improve microbial fermentation performance (Lee et al., 2022), often beyond what can be achieved with equivalent concentrations of analytical-grade sugars. Such enhancements are attributed to complex and poorly characterized medium components present in biosugars. We used biosugars as natural test cocktails to identify potential medium intensification factors that could contribute to productivity improvement. To examine whether such effects also apply to theanine production, we tested recombinant *C. glutamicum* KCTC 1852 bioprocess using biosugars derived from SSB (Fig. 3a). SSB was subjected to hydrothermal pretreatment, followed by enzymatic hydrolysis, to prepare SSB-derived biosugars. The composition of SSB before and after refining is summarized in Fig. 3b and 3c, and the detailed pretreatment/refining/saccharification procedures and results are described in supplementary materials. To prepare cultivation media containing approximately 30 g/L total sugars, enzymatic hydrolysis was conducted under various glucan loadings and enzyme dosages. The sugar release profiles used to select the hydrolysate conditions are summarized in Fig. 3d and 3e, with full screening details provided in supplementary materials. Based on sugar release efficiency and process practicality, hydrolysis at 10% glucan loading with 20 FPU was selected to prepare the CG30 medium for subsequent cultivation experiments. The resulting hydrolysate was applied to the theanine biosynthesis system using recombinant strains THE-4 and THE-6. To assess their ability to utilize SSB-derived sugars, both strains were cultivated in (i) CG30 medium supplemented with analytical-grade sugars, glucose, and mixed sugars (xylose, galactose, and mannose; XGM), and (ii) CG30 medium prepared with saccharified SSB hydrolysate (Mao et al., 2018). Sugar concentrations in CG30 were adjusted to match those in the hydrolysate (166.2 mM glucose and 14.6 mM xylose). Both strains produced more theanine in the biosugar-containing medium than CG30 with analytical-grade sugars. THE-4 and THE-6 exhibited 1.38- and 1.48-fold increases in theanine titer, respectively (Fig. 3f). Additional nutrients present in the SSB hydrolysate may contribute to enhanced theanine biosynthesis in *C. glutamicum*. To evaluate whether the productivity improvement observed with the SSB hydrolysate was attributable to XGM (specifically xylose), the cultivation conditions were adjusted to a total sugar concentration of 30 g/L: (i) glucose 30 g/L, (ii) xylose 30 g/L, and (iii) glucose 28 g/L with xylose 2 g/L. Accordingly, theanine concentrations were 25.44 mM (4.38 g/L), 7.52 mM (1.31 g/L), and 26.37 mM (4.59 g/L), respectively (Fig. 3g, supplementary materials). The corresponding yields were 0.153, 0.038, and 0.156 mM/mM for glucose-only, xylose-only, and mixed-sugar conditions, respectively. Compared to glucose alone, cultivation on xylose as the sole carbon source resulted in substantially lower theanine productivity, while minor xylose supplementation (2 g/L) produced titers and yields comparable to glucose-only conditions. Thus, under the tested carbon ratio, xylose neither enhanced productivity nor imposed detectable carbon catabolite repression. As previously reported (Kawaguchi et al., 2006), wild-type *C. glutamicum* lacks the native ability to metabolize xylose. To confirm functional implementation of the *xylA*/*xylB* module, sugar utilization profiles were analyzed under xylose-containing conditions. Time-course measurements demonstrated progressive xylose consumption, with substantial depletion observed within 48 h. Under mixed-sugar conditions, glucose and xylose were simultaneously consumed, and OD_{600} increased over time, confirming effective co-utilization and growth supported by xylose (see supplementary materials). Collectively, these results validate the functional assimilation of xylose enabled by the introduced *xylA* and *xylB* genes while demonstrating that glucose–xylose interactions did not account for the enhanced theanine production observed in biosugar media.

3.3. Identification of the primary factor enhancing theanine production in biosugars

Although cultivation with SSB-derived biosugars improves theanine production, the underlying biochemical factors responsible for this enhancement remain unclear. To identify which components within the biosugar medium contributed to enhanced productivity, an untargeted compositional analysis was conducted using GC–MS, comparing the biosugar medium with the CG30 medium formulated with analytical-grade sugars (Fig. 4a). Citrate was subsequently identified as a candidate productivity-enhancing factor. To more clearly define the specific effect of citrate, validation experiments were performed under glucose-based cultivation conditions. By excluding mixed carbon sources during validation, this design enabled isolation of the citrate-specific contribution to productivity enhancement. GC–MS data were analyzed using OPLS-DA to assess the compositional differences between the two media. The model showed a clear separation along the first predictive component (t[1]), which explained 46.6% of the X-variance (R^2X = 0.466; Fig. 4b) with strong explanatory and predictive performance (R^2Y

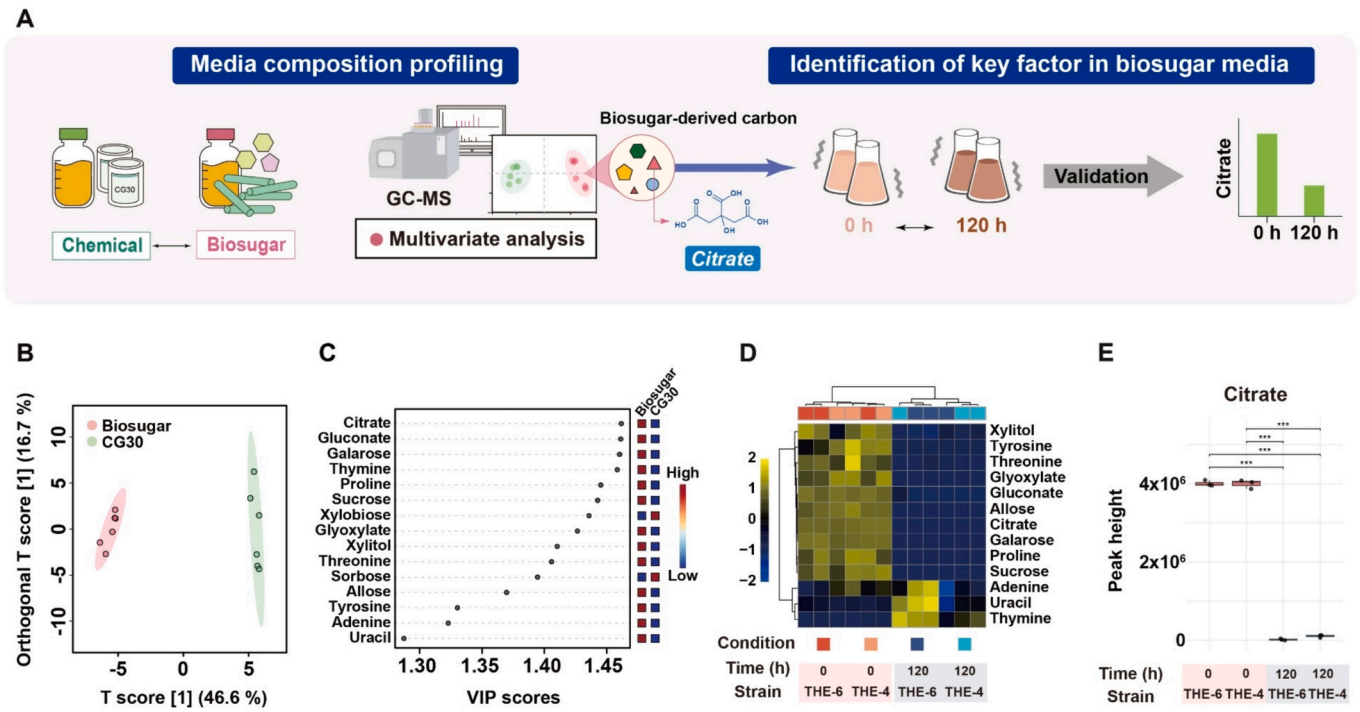


Fig. 4. Identification of citrate as a key factor in biosugar medium for theanine production. **(A)** Schematic overview of GC–MS-based profiling to identify key factors in biosugar medium. **(B)** OPLS-DA score plot showing separation between biosugar-supplemented and CG30 media ($n = 6$). **(C)** VIP score plot of the top 15 discriminating compounds (VIP ≥ 1) with relative abundances. **(D)** HCA of temporal abundance patterns (0–120 h) for compounds enriched in biosugar-supplemented media ($n = 3$). **(E)** Box plot showing significant depletion of citrate after 120 h of cultivation. Data represent individual values with median and interquartile ranges ($n = 3$). GC–MS, gas chromatography–mass spectrometry; VIP, variable importance in projection; OPLS-DA, orthogonal partial least squares discriminant analysis; HCA, hierarchical cluster analysis.

$= 0.987$, $Q^2 = 0.963$). Model robustness was confirmed by permutation testing ($n = 1{,}000$, $p = 0.003$). Key contributors to the separation were identified using VIP score analysis, which revealed several discriminant compounds (Fig. 4c). Citrate exhibited the highest VIP score, followed by gluconate, galarose, thymine, proline, and sucrose. Notably, citrate was absent in both raw and pretreated SSB but was detected in the enzymatic hydrolysate. This suggests a process-derived origin and prompted an investigation into its potential role in the observed enhancement. The compound was added to the citrate buffer used during saccharification. The citrate concentration in CG30 (48.24 mM) corresponded to the 2.5-fold dilution of citrate buffer used during saccharification (121.33 mM). To assess metabolic relevance, culture supernatants were compared before (0 h) and after (120 h) cultivation. Most biosugar-enriched compounds, including citrate, gluconate, galarose, threonine, and tyrosine, decreased after fermentation (Fig. 4d), indicating their use by recombinant strains THE-4 and THE-6. Comparing the base peak heights before and after cultivation confirmed a substantial reduction of citrate (Fig. 4e), demonstrating active consumption during fermentation. Thus, citrate functions as a bioprocess-enhancing factor, facilitating the redistribution of carbon flux toward the theanine biosynthetic route. Citrate, originating from the saccharification buffer system, was detected as a discriminant component in the biosugar medium and subsequently validated as a productivity-enhancing factor through controlled supplementation experiments.

3.4. Synergistic effect of citrate supplementation on theanine production and carbon yield

To validate the role of citrate as a bioprocess-enhancing factor, *C. glutamicum* THE-4 and THE-6 strains were cultivated in CG30 medium supplemented with citrate at various concentrations. Citrate increased theanine production in both strains, with a stronger response observed in THE-6. Theanine titers increased in a citrate concentration-dependent manner, reaching a maximum of 82.26 mM (14.33 g/L) at 400 mM citrate, corresponding to a 3.29-fold increase relative to the CG30 condition (Fig. 5a). As citrate was identified in the biosugar-based CG30 medium at a concentration of approximately 50 mM (Section 3.3), this concentration was selected to evaluate the functional role of citrate under biosugar-mimicking conditions. Owing to their superior responsiveness to citrate supplementation, THE-6 was selected for subsequent analysis. To determine whether citrate exerts effects beyond serving as an additional carbon source, time-course profiles of key substrates and metabolites were compared under carbon-equivalent conditions: CG39 (216.8 mM glucose, 39 g/L) versus $CG30_{cit50}$ (166 mM glucose, 30 g/L; 50 mM citrate, 9.6 g/L). A citrate concentration of 50 mM was selected to match the citrate level detected in the biosugar-based CG30 medium (48.24 mM; Section 3.3), enabling biosugar-mimicking evaluation under carbon-equivalent conditions. Under these conditions, THE-6 produced 1.86-fold and 2.24-fold higher theanine titers in $CG30_{cit50}$ than in CG39 medium at 12 h and 21 h, respectively, reaching 37.21 mM (6.48 g/L) at 72 h (Fig. 5c and 5d). Notably, these experiments were performed under carbon-equivalent conditions to distinguish citrate-mediated metabolic reinforcement from simple carbon supplementation effects. The observed improvements in theanine titer and yield under equal total carbon supply indicate that citrate functions beyond serving as an auxiliary carbon source. In addition to enhanced theanine production, lactate accumulation was reduced in the citrate-supplemented cultures. Lactate concentrations reached 7.43 mM in the CG39 medium but only 4.9 mM in $CG30_{cit50}$, suggesting improved redirection of carbon flux toward oxidative metabolism.

Citrate upregulates the expression of several TCA cycle–associated genes, including those encoding aconitase, succinyl-CoA synthetase, succinate dehydrogenase, fumarase, and subunits of the F_0F_1 ATP synthase complex (Polen et al., 2007). Therefore, enhanced TCA cycle activity is expected to increase the intracellular ATP availability. To

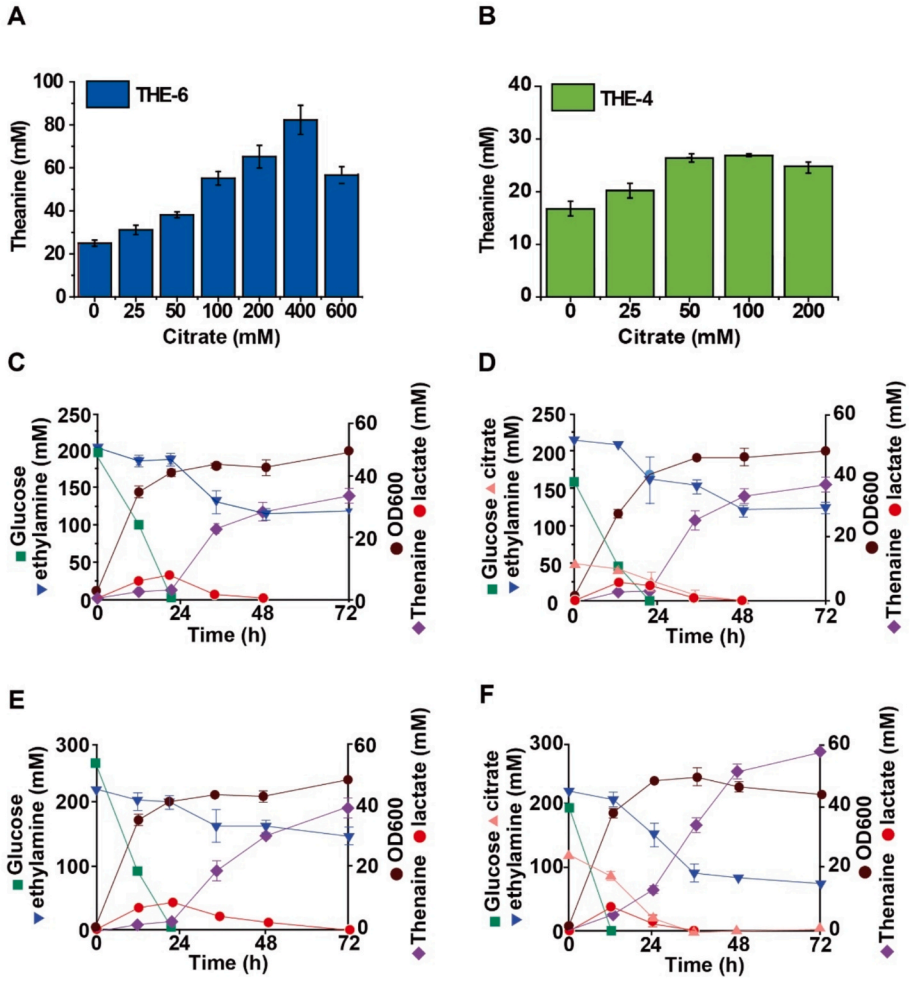


Fig. 5. Effect of citrate on theanine production. **(A, B)** Concentration-dependent effects of citrate on theanine production in THE-6 and THE-4. **(C–F)** Time-course profiles of glucose, ethylamine, citrate, theanine, lactate, and cell growth (OD_{600}) during theanine production under **(C)** CG39, **(D)** CG30 supplemented with 50 mM citrate, **(E)** CG48, and **(F)** CG30 supplemented with 100 mM citrate. OD, optical density.

Table 2
Effects of citrate supplementation on product titers and yields in engineered *C. glutamicum* strains.

Strain	Target product	Key cofactor	Medium	Titer (mM)	Yield (mM/mM)	Yield (g/g)
THE-4	Theanine	ATP	$CG30_{cit50}$	18.46	0.07	0.08
			CG39	22.25	0.07	0.09
THE-6	Theanine	ATP	$CG30_{cit50}$	37.21	0.09	0.13
			$CG30_{cit100}$	57.31	0.11	0.18
			CG39	33.38	0.08	0.12
			CG48	39.43	0.08	0.12
LYS	Lysine	NADH	$CG30_{cit50}$	111.19	0.44	0.42
			CG39	75.98	0.31	0.28
HV	5-Hydroxyvaleric acid (5-HV)	NAD(P)H	$CG30_{cit50}$	20.93	0.08	0.06
			CG39	8.12	0.03	0.02
GTA	Glutarate	$NAD(P)^+$	$CG30_{cit50}$	65.62	0.27	0.22
			CG39	44.36	0.19	0.15
*C. glutamicum*PKC	Lysine	NADPH	$CG30_{cit50}$	82.25	0.34	0.31
			CG39	71.19	0.31	0.27

examine whether elevated ATP availability could differentially influence the catalytic steps of theanine biosynthesis, the ATP-binding interactions of EcGCS and MmGMAS were analyzed by molecular docking simulations (see supplementary materials). Consistent with these observations, increasing citrate concentrations beyond 50 mM further improved the theanine titer and yield to 57.31 mM (9.98 g/L) and 0.11 mM/mM, respectively, in CG30 medium supplemented with 100 mM citrate (i.e., $CG30_{cit100}$ medium) (Fig. 5e, 5f and Table 2), indicating that the productivity-enhancing effect of citrate is not restricted to a single concentration but persists across a defined supplementation range. When normalized to the total carbon supplied (glucose, ethylamine, and citrate), the theanine yield in citrate-supplemented CG medium increased compared with that in CG medium containing an equivalent amount of glucose (Table 2). These results demonstrate that citrate enhances theanine productivity and carbon use efficiency beyond its contribution as an additional carbon source, thus validating its role as a

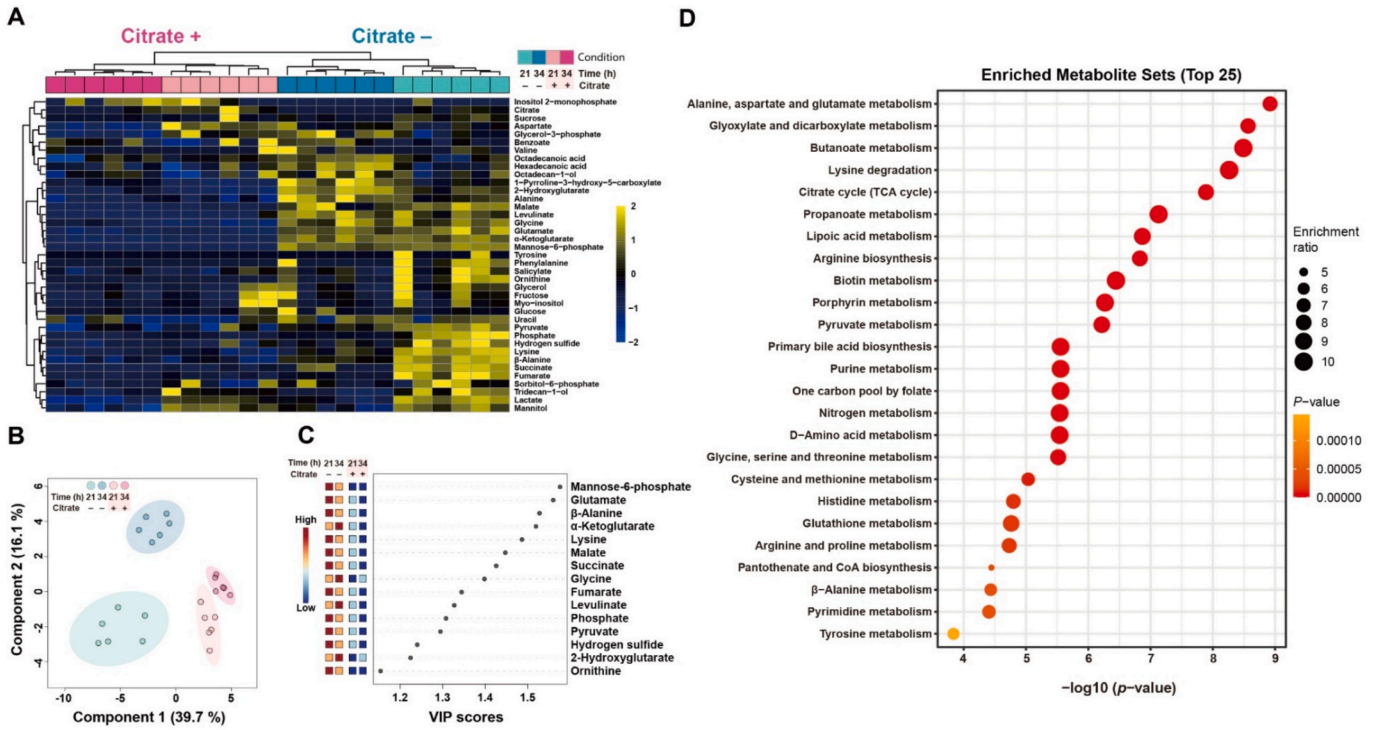


Fig. 6. Intracellular metabolomic response of strain THE-6 to citrate supplementation. **(A)** HCA of intracellular metabolites in citrate − and citrate + cultures at 21 h and 34 h. **(B)** PLS-DA score plot comparing citrate − and citrate + conditions. **(C)** VIP scores of major discriminant metabolites (VIP > 1). **(D)** MSEA showing enriched metabolite sets at 21 h under citrate − and citrate + conditions. Analyses were performed using six independent biological replicates per condition. HCA, hierarchical cluster analysis; PLS-DA, partial least squares discriminant analysis; VIP, variable importance in projection; MSEA, metabolite set enrichment analysis.

biosugar-derived media-intensification factor. Although the maximum titer obtained in this study (14.33 g/L) is lower than those reported in state-of-the-art systems, where L-theanine titers exceeding 40 g/L have been achieved in optimized fed-batch processes and 15–20 g/L in shake-flask cultures through extensive strain engineering (Yang et al., 2024), it was achieved solely through medium-level modulation without additional strain engineering. Importantly, under carbon-equivalent conditions, citrate supplementation resulted in up to ~ 1.5-fold higher theanine titers when compared to glucose-only controls. This relative enhancement highlights the specific contribution of targeted medium intensification, independent of further genetic optimization, in improving theanine production.

3.5. Metabolic changes induced by citrate supplementation

To investigate the citrate-driven enhancement of theanine production, we conducted GC–MS-based intracellular metabolite profiling of *C. glutamicum* THE-6, a strain that responds strongly to citrate. Sampling was performed at 21 h and 34 h, representing the early and active theanine-producing phases, respectively. HCA, an unsupervised approach that groups samples based on overall similarity in metabolic profiles, indicated a clear separation between the citrate-supplemented and no-citrate control conditions (Fig. 6a). This separation was more pronounced than the differences observed between the fermentation time points, which indicated that citrate exerted a stronger influence on the intracellular metabolic landscape than fermentation time (Fig. 6a). Within each condition, samples collected at 21 and 34 h were further differentiated, suggesting that time-dependent metabolic changes accompanied the transition toward theanine production. Most of the 39 detected metabolites were more abundant in the no-citrate control cultures, whereas citrate supplementation led to decreases, implying faster metabolic turnover and enhanced carbon flux toward energy and amino acid metabolism (Fig. 6a). PLS-DA was used to examine the relative contributions of citrate supplementation and fermentation time to these metabolic differences. This analysis enabled a comparison of global metabolic patterns between citrate-supplemented and no-citrate control conditions while accounting for time-dependent variations. The PLS-DA score plot showed a clear differentiation of the samples, primarily along component 1 (39.7% of the variance) by citrate supplementation and secondarily along component 2 (16.1%) by fermentation time (Fig. 6b). These results indicate that citrate induces a distinct metabolic state, whereas fermentation time reflects the progression toward the theanine-producing phase. The PLS-DA model performance was assessed by cross-validation ($R^2 = 0.93$ and $Q^2 = 0.77$). Permutation testing ($n = 1{,}000$) supported the statistical significance of the model ($p = 0.001$). VIP score analysis identified α-ketoglutarate, malate, glutamate, alanine, and glycine as the most influential metabolites contributing to group differentiation (Fig. 6c). These compounds are primarily involved in the TCA cycle and amino acid metabolism. Their reduced abundance under citrate-supplemented conditions likely reflects an accelerated turnover through oxidative metabolic pathways. MSEA further supported these results, highlighting the TCA cycle, glyoxylate, dicarboxylate metabolism, and alanine/aspartate/glutamate metabolism as the most affected pathways (Fig. 6d; see supplementary materials). This suggests broad activation of oxidative and nitrogen-related metabolic networks by citrate supplementation.

3.6. Integrated metabolic, transcriptional, and energetic responses associated with enhanced theanine production

To further link metabolic shifts with gene expression, transcriptional profiling was conducted for key genes involved in carbon entry into the TCA cycle, oxidative flux through the central metabolism, NADH oxidation, and lactate and theanine formation (Fig. 7). The expression levels of *acn*, *icd*, *odhA*, *sucD*, *mqo*, and *gltA* in the TCA cycle were upregulated under citrate supplementation, particularly at 34 h. In addition to these TCA cycle genes, the expression levels of *aceF*, *gdh*, *ndh*, and *ldhA* were quantified to assess citrate-associated changes in

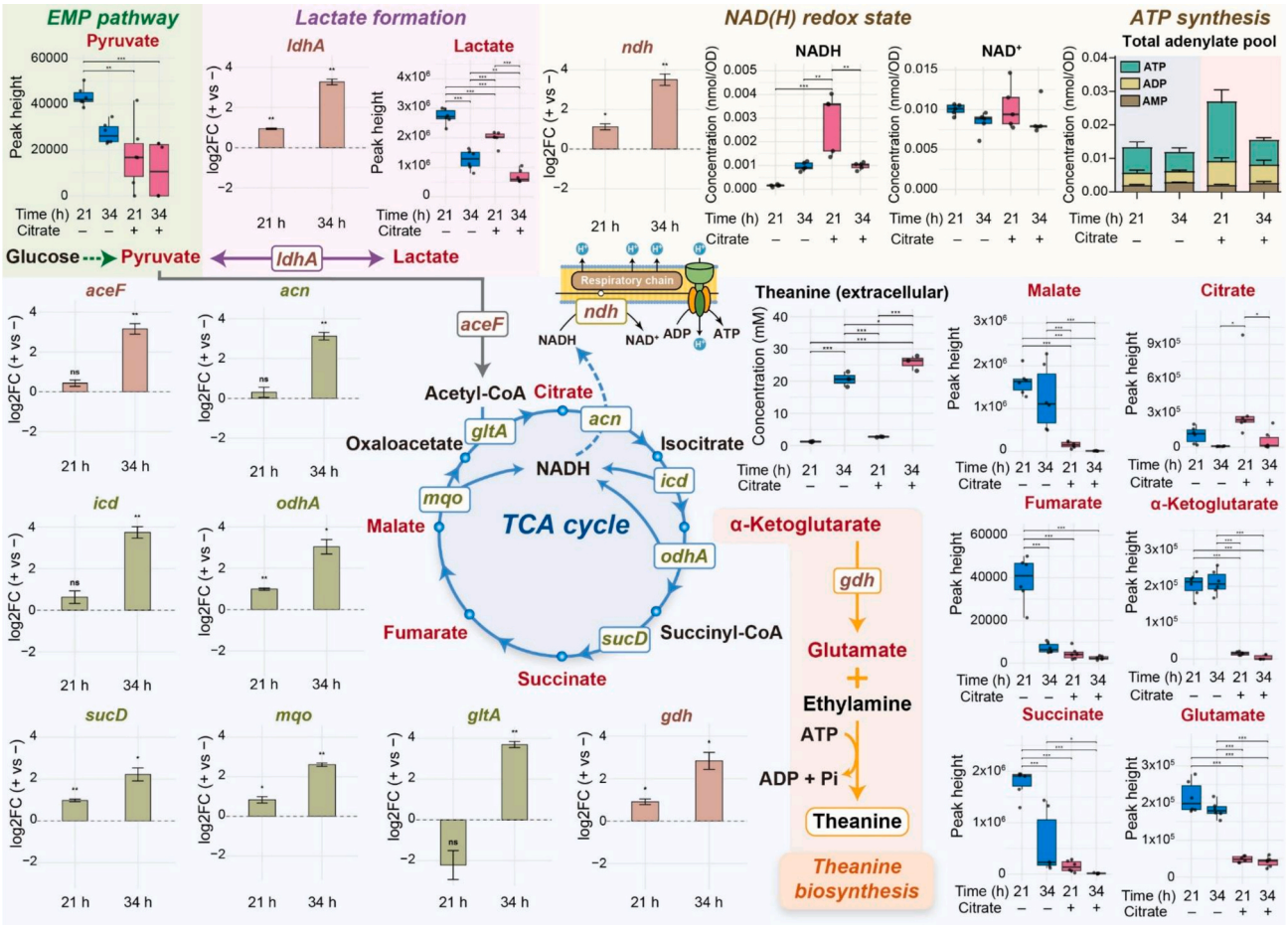


Fig. 7. Citrate-driven metabolic rewiring enhances energy metabolism and theanine production. Pathway map summarizes citrate-dependent changes in intracellular metabolites, gene expression, and theanine production in THE-6 cultures at 21 h and 34 h. Intracellular metabolites showing significant changes by GC–MS are highlighted in red; extracellular theanine was quantified in the supernatant by HPLC. NADH and NAD^+ were quantified by LC-MS/MS. Differences between citrate − and citrate + groups were assessed by ANOVA followed by Tukey's HSD test, with significance annotated as * (adjusted $p < 0.05$), ** (adjusted $p < 0.01$), and *** (adjusted $p < 0.001$). Box plots show individual data points with the median and interquartile range (intracellular metabolites, $n = 6$ per group; extracellular metabolites, $n = 3$ per group; NADH and NAD^+, $n = 5$ per group). qPCR-based gene expression is presented as the $\log_2$ fold change ($\log_2$FC) relative to citrate−; genes validated by qPCR are indicated in olive green. TCA cycle-related genes are shown in olive green, and all other genes in rosy brown. Error bars represent mean ± standard error of the mean (SEM) from three independent biological replicates. Significance of $\log_2$FC was evaluated by a one-sample *t*-test against 0 ($\log_2$FC = 0) and annotated as ns ($p \geq 0.05$), * ($p < 0.05$), ** ($p < 0.01$), and *** ($p < 0.001$) using raw *p*-values. Intracellular adenylates (ATP, ADP, AMP) were quantified at 21 h and 34 h in citrate − and citrate + cultures; concentrations are presented as the mean ± SD ($n = 4$). GC–MS, gas chromatography–mass spectrometry; HPLC, high-performance liquid chromatography; LC-MS/MS, liquid chromatography–tandem mass spectrometry; ANOVA, one-way analysis of variance; HSD, honest significant difference; qPCR, quantitative polymerase chain reaction; SD, standard deviation; EMP, Embden–Meyerhof–Parnas; TCA, tricarboxylic acid.

pyruvate-derived carbon entry into the TCA cycle, glutamate metabolism, respiratory NADH oxidation, and lactate formation. This transcriptional upregulation temporally corresponded with a reduction of central carbon/TCA-cycle intermediates, including pyruvate, α-ketoglutarate, succinate, fumarate, and malate, which is consistent with enhanced oxidative flux and/or increased turnover of TCA cycle intermediates rather than their accumulation (Fig. 7). Lower lactate levels ($q < 0.05$), despite *ldhA* upregulation to 9.74-fold at 34 h under citrate supplementation, are consistent with a relative decrease in fermentative lactate formation, with intracellular redox balance likely supported mainly through oxidative metabolism (Fig. 7). The respiratory NADH dehydrogenase gene *ndh* was significantly upregulated by citrate supplementation to 11.75-fold at 34 h ($p < 0.05$), consistent with enhanced NADH oxidation through the respiratory chain rather than fermentative pathways (Fig. 7). Furthermore, since LdhA has been reported to catalyze a reversible reaction (pyruvate ↔ lactate), transcriptional changes in *ldhA* may not necessarily translate into proportional changes in intracellular lactate levels (Sharkey et al., 2011). In this context, the coordinated decrease in pyruvate and lactate, together with activation of TCA cycle–associated genes and increased ATP availability, suggests that these patterns are consistent with a redistribution of carbon flux toward oxidative metabolism rather than net lactate accumulation.

At 21 h, citrate supplementation was associated with increased intracellular NADH levels and enhanced ATP generation, consistent with an elevated energy-producing state during the growth phase (Fig. 7). Notably, intracellular NADH levels increased by 18.53-fold under citrate supplementation compared with the control at this time point (Fig. 7). This was accompanied by an increased NADH/NAD^+ ratio (see supplementary materials) and decreased intracellular levels of several TCA cycle intermediates, including α-ketoglutarate, succinate, fumarate, and malate (Fig. 7), suggesting enhanced TCA turnover rather than metabolite accumulation. In contrast, at 34 h, differences in intracellular NADH, ATP levels, and the NADH/NAD^+ ratio between conditions were not pronounced, whereas a clear difference was observed in theanine production (Fig. 7). These results suggest that early-phase changes in cellular redox and energy status were temporally associated with enhanced theanine production at the later time point. Consistent with enhanced oxidative metabolism, citrate supplementation increased the

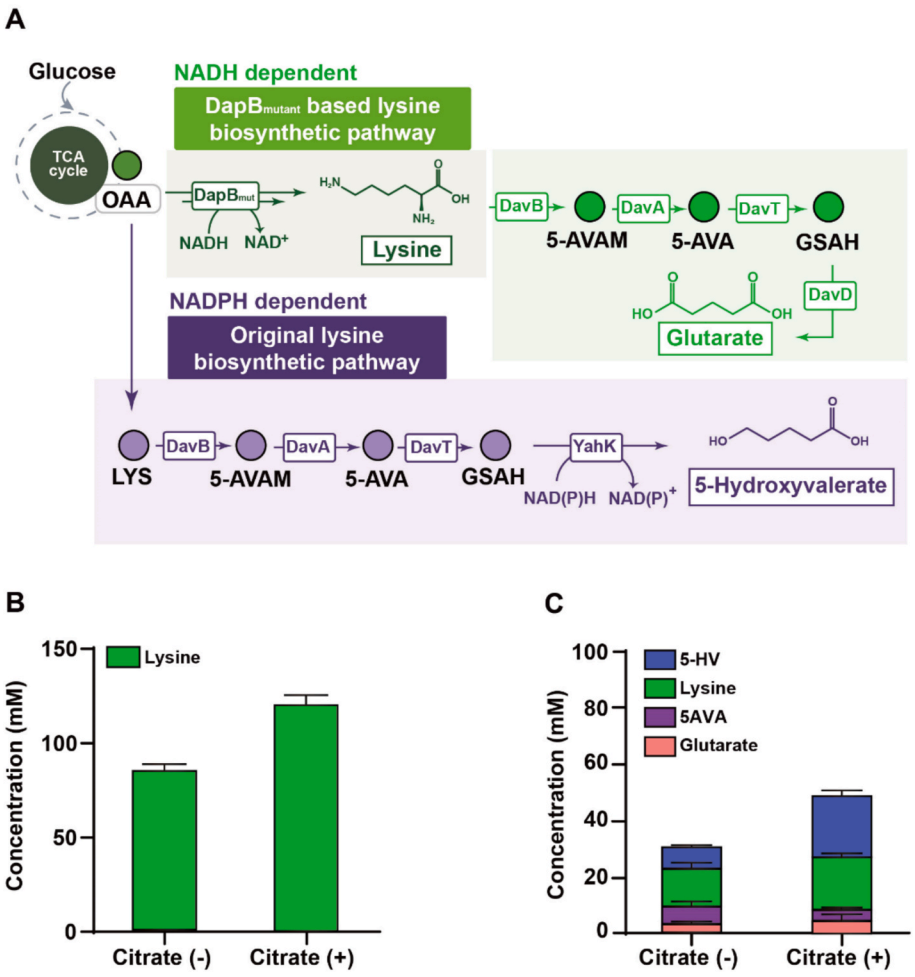


Fig. 8. Citrate-enhanced production of lysine and lysine-derived compounds via an NADH-dependent pathway. **(A)** Schematic of an engineered NADH-dependent lysine biosynthesis pathway and its extension to glutarate and 5-hydroxyvalerate, compared with the native NADPH-dependent route. **(B)** Lysine production in strain LYS via the NADH-dependent pathway under citrate-free and citrate-supplemented conditions. **(C)** Production of lysine and lysine-derived metabolites in strain HV under citrate-free and citrate-supplemented conditions.

intracellular ATP from 0.0072 nmol/OD to 0.0181 nmol/OD at 21 h (Fig. 7) and from 0.006 nmol/OD to 0.0075 nmol/OD at 34 h (Fig. 7). Similarly, the total adenylate pool (ATP + ADP + AMP) increased under citrate supplementation at both time points. In contrast, the adenylate energy charge remained largely unchanged, indicating that improved ATP availability was achieved without perturbing overall energy homeostasis (Fig. 7). Enhanced theanine biosynthesis occurred without targeted analysis of theanine biosynthetic gene expression, suggesting that increased production was primarily driven by improved energetic and redox states rather than the transcriptional upregulation of downstream product-specific enzymes. Levels of intracellular glutamate, a direct precursor of theanine, decreased with citrate supplementation. Moreover, extracellular theanine accumulation was increased, indicating efficient conversion (Fig. 7). In contrast, citrate-free conditions led to glutamate accumulation (Fig. 7), which is consistent with the limited energetic or redox capacity to sustain glutamate-to-theanine conversion. Overall, the integrated metabolic and transcriptional responses indicate that citrate supplementation does not merely serve as an auxiliary carbon source, but rather functions as a medium-level metabolic reinforcement lever that systemically enhances oxidative flux, ATP regeneration, and redox balance. This conceptually differs from conventional metabolic engineering strategies that rely primarily on intracellular enzyme overexpression or cofactor regeneration modules. In this context, citrate supplementation modulates cellular energetic and redox states without direct modification of intracellular pathway architecture.

3.7. *Expanding and validating citrate-mediated enhancement in NADH-dependent biosynthetic pathways*

In theanine biomanufacturing, citrate supplementation enhanced production by increasing the intracellular ATP pool. Since this ATP elevation resulted from enhanced oxidative TCA cycle flux, which simultaneously generates NADH at multiple dehydrogenase steps (Fig. 7), we hypothesized that citrate supplementation could also reinforce NADH-dependent biosynthetic pathways. In support of this possibility, intracellular NADH levels and NADH/NAD^+ ratios were directly quantified and were found to increase under citrate-supplemented conditions (Fig. 7). Accordingly, we evaluated its effect on representative NADH-dependent chemicals, including lysine and its derivative glutaric acid, as well as 5-hydroxyvalerate (5-HV), by examining their respective production pathways (Fig. 8a, Table 2). For consistency, citrate was supplemented at 50 mM in all lysine, glutaric acid, and 5-HV cultivation experiments. Cell growth was monitored as OD_{600}, and no significant differences in biomass were observed under citrate-supplemented conditions, indicating that productivity enhancement

was not attributable to increased cell growth. Furthermore, although citrate supplementation increased product titers across all tested pathways, the magnitude of enhancement was more pronounced in the NADH-dependent lysine ($DapB_{mut}$) and 5-HV pathways than in their native configurations, supporting the role of citrate in reinforcing intracellular redox metabolism. In the lysine pathway, the native NADPH-dependent DapB was replaced with an engineered NADH-dependent mutant ($DapB_{mut}$), enabling pathway extension toward glutaric acid (Sohn et al., 2022). In the 5-HV pathway, YahK, with a dual cofactor preference (NAD(P)H), catalyzes the conversion of glutarate semialdehyde to 5-HV (Fig. 8a) (Sohn et al., 2025). To examine whether citrate supplementation improved titers in an NADH-dependent biosynthetic route, we first evaluated the effect of $DapB_{mut}$ expression in the lysine-overproducing *C. glutamicum* PKC strain. When cultivated in $CG30_{cit50}$ medium, the $DapB_{mut}$-expressing strain produced 111.19 mM (16.26 g/L) lysine, compared with 75.98 mM (11.11 g/L) in CG39. The yield also increased from 0.31 mM/mM to 0.44 mM/mM on a total carbon basis, indicating that citrate supplementation enhanced both productivity and carbon conversion efficiency (Table 2). To clarify whether this enhancement originated from increased NADH availability or citrate-driven expansion of the oxaloacetate pool, the parental *C. glutamicum* PKC strain was cultivated with and without citrate. In the parental strain, citrate supplementation increased lysine production from 71.19 mM to 82.25 mM (1.16-fold). In contrast, citrate supplementation increased lysine production in the $DapB_{mut}$-expressing strain by 1.41-fold (Fig. 8b). The greater improvement observed specifically in the NADH-dependent strain indicates that citrate supplementation preferentially enhances reducing-equivalent availability rather than merely increasing aspartate-derived precursor flux. (Fig. 8b, supplementary materials). This interpretation is consistent with the experimentally observed increase in intracellular NADH levels and NADH/NAD^+ ratios under citrate supplementation (Fig. 7, supplementary materials). Next, we evaluated whether this improvement in lysine availability was extended to the downstream glutaric acid branch. When the GTA strain was cultivated in $CG30_{cit50}$, glutaric acid production showed a 1.48-fold increase upon citrate supplementation compared to cultures in CG39 (see supplementary materials). This is most likely attributable to the enlarged lysine pool generated by citrate-enabled intensification, which increases the availability of precursors for glutarate biosynthesis. To further investigate whether citrate can support more demanding NADH-dependent steps, we examined the lysine-derived 5-HV pathway, which requires one mole of reducing equivalent and exhibits dual NADPH/NADH preference. Citrate supplementation increased the 5-HV titer from 8.12 to 20.93 mM, with a corresponding improvement in carbon yield from 0.03 to 0.08 mM/mM. These results suggest that citrate sustained a higher reducing equivalent flux, enabling more robust downstream conversion relative to the non-supplemented control (Fig. 8c). Although YahK accepts both NADPH and NADH, the observed enhancement indicates that increased NADH availability alone is sufficient to drive the reductive step in vivo under citrate-supplemented conditions. Consistent with the observed increase in intracellular NADH levels and NADH/NAD^+ ratios, the preferential improvement in strains containing NADH-dependent steps further supports the contribution of enhanced reducing-equivalent availability to increased product titers. Taken together, these findings integrate citrate supplementation into a broader framework of metabolic reinforcement, in which citrate acts not only as an ATP-supporting supplement but also as a medium-level modulator of intracellular energy and redox metabolism, as supported by increased intracellular ATP and NADH levels under citrate supplementation.

Overall, these findings indicate that citrate supplementation supports both ATP-intensive and NADH-dependent biosynthesis by reinforcing intracellular energy and reducing-equivalent availability. Although the maximum titer achieved in this study is lower than that of fully optimized fed-batch systems, the enhancement was achieved solely through medium-level intervention without further strain engineering. Therefore, the present work should be interpreted as a proof-of-concept demonstration of medium-driven metabolic reinforcement rather than a fully optimized production system. Further fermentation optimization, scale-up, and techno-economic analysis are required to evaluate industrial feasibility.

4. Conclusion

Here, we present a citrate-enabled process intensification strategy that enhances sustainable L-theanine bioproduction in *C. glutamicum*. Recombinant strains expressing heterologous theanine synthases efficiently converted SSB-derived biosugars to L-theanine, with THE-6 (EcGCS) showing the highest productivity. Metabolomic screening identified citrate as a key productivity-enhancing component, and controlled supplementation significantly improved theanine titers and carbon yields, while reducing lactate overflow at 34 h ($p < 0.05$) (Fig. 7). Integrated analyses revealed a system-wide metabolic response, in which citrate strengthened TCA cycle activity, increased intracellular ATP availability, and promoted efficient glutamate use. This intensification effect was further extended to NADH-dependent pathways, including lysine and 5-HV production, demonstrating its broader applicability across energy- and redox-demanding bioconversions. Overall, citrate supplementation offers a simple and effective medium-level intervention that complements metabolic engineering and supports the production of amino acids and related biochemicals from biomass-derived sugars. This proof-of-concept study provides an important foundation for future integration of strain engineering and precision fermentation.

CRediT authorship contribution statement

KwangYoung Park: Writing – original draft, Visualization, Validation, Methodology, Investigation, Formal analysis, Data curation. **Hoe-Suk Lee:** Writing – original draft, Visualization, Validation, Methodology, Investigation, Formal analysis, Data curation. **Dong Young Lee:** Writing – original draft, Visualization, Validation, Software, Methodology, Investigation, Formal analysis, Data curation. **June-Ho Choi:** Validation, Methodology, Investigation, Data curation. **Yunhee Jeong:** Validation, Methodology, Investigation, Data curation. **SunJoo Park:** Validation, Methodology, Investigation, Data curation. **Yunjeong Song:** Validation, Methodology, Investigation, Data curation. **Jiyoung Park:** Validation, Methodology, Investigation, Data curation. **Chan-Duck Jung:** Validation, Methodology, Data curation. **Hoyong Kim:** Validation, Methodology, Investigation, Data curation. **Sung-Hyun Jo:** Validation, Software, Methodology, Investigation, Data curation. **Yun-Gon Kim:** Software, Methodology, Data curation. **Yung-Hun Yang:** Validation, Methodology, Data curation. **See-Hyoung Park:** Validation, Methodology, Data curation. **Kyungmoon Park:** Validation, Methodology, Data curation. **Si Jae Park:** Validation, Methodology, Data curation. **Jungoh Ahn:** Validation, Methodology, Data curation. **Eun Ju Yun:** Writing – review & editing, Writing – original draft, Supervision, Resources, Project administration, Conceptualization. **Young Joo Yeon:** Writing – review & editing, Writing – original draft, Supervision, Resources, Project administration, Conceptualization. **Hee Taek Kim:** Writing – review & editing, Writing – original draft, Supervision, Resources, Project administration, Funding acquisition, Conceptualization.

Funding

This research was supported by the Korea Evaluation Institute of Industrial Technology (KEIT) R&D Program (20025698 and 20018337) and a National Research Foundation of Korea (NRF) grant funded by the Korean government (MSIT) (RS-2024-00341995, RS-2024-00439872, RS-2025-24535664, and RS-2024-00452695).

Declaration of competing interest

The authors declare that they have no known competing financial interests or personal relationships that could have appeared to influence the work reported in this paper.

Acknowledgments

The authors gratefully acknowledge financial support from the Korea Evaluation Institute of Industrial Technology (KEIT) R&D Program (Nos. 20025698 and 20018337) and the National Research Foundation of Korea (NRF), funded by the Ministry of Science and ICT (MSIT).

Appendix A. Supplementary data

Supplementary data to this article can be found online at https://doi.org/10.1016/j.biortech.2026.134464.

Data availability

Data will be made available on request.

References

Akiyama, M., Osanai, T., 2024. Regulation of organic acid and hydrogen production by NADH/NAD^+ ratio in *Synechocystis* sp. PCC 6803. Front. Microbiol. 14, 1332449. https://doi.org/10.3389/fmicb.2023.1332449.

Chang, Z., Dai, W., Mao, Y., Cui, Z., Wang, Z., Chen, T., 2020. Engineering *Corynebacterium glutamicum* for the efficient production of 3-hydroxypropionic acid from a mixture of glucose and acetate via the malonyl-CoA pathway. Catalysts 10, 203. https://doi.org/10.3390/catal10020203.

Chen, J., Li, W., Zhang, Z.-Z., Tan, T.-W., Li, Z.-J., 2018. Metabolic engineering of *Escherichia coli* for the synthesis of polyhydroxyalkanoates using acetate as a main carbon source. Microb. Cell Fact. 17, 102. https://doi.org/10.1186/s12934-018-0949-0.

Cho, D.H., Kim, S., Lee, Y., Shin, Y., Choi, S., Oh, J., Kim, H.T., Park, S.-H., Park, K., Bhatia, S.K., 2024. Enhanced theanine production with reduced ATP supply by alginate entrapped *Escherichia coli* co-expressing γ-glutamylmethylamide synthetase and polyphosphate kinase. Enzyme Microb. Technol. 175, 110394. https://doi.org/10.1016/j.enzmictec.2024.110394.

Han, X., Li, L., Wei, C., Zhang, J., Bao, J., 2019. Facilitation of L-lactic acid fermentation by lignocellulose biomass rich in vitamin B compounds. J. Agric. Food Chem. 67, 7082–7086. https://doi.org/10.1021/acs.jafc.9b02297.

Jeong, Y., Kim, Y., Kim, K.-A., Sohn, Y.J., Park, K., Song, E., Park, K., Park, S.-H., Yang, Y.-H., Choi, J.H., 2025. Development of scalable precision fermentation and chemical-grade purification of 5-aminovaleric acid for high-value valorization. Chem. Eng. J. 168950. https://doi.org/10.1016/j.cej.2025.168950.

Kawaguchi, H., Vertès, A.A., Okino, S., Inui, M., Yukawa, H., 2006. Engineering of a xylose metabolic pathway in *Corynebacterium glutamicum*. Appl. Environ. Microbiol. 72, 3418–3428. https://doi.org/10.1128/AEM.72.5.3418-3428.2006.

Kim, S., Hwang, J., Kim, J., Ahn, J.K., Cha, H.-S., Kim, K.H., 2017. Metabolite profiles of synovial fluid change with the radiographic severity of knee osteoarthritis. Joint Bone Spine 84, 605–610. https://doi.org/10.1016/j.jbspin.2016.05.018.

Kopka, J., Schauer, N., Krueger, S., Birkemeyer, C., Usadel, B., Bergmüller, E., Dörmann, P., Weckwerth, W., Gibon, Y., Stitt, M., 2005. GMD@ CSB. DB: the Golm metabolome database. Bioinformatics 21, 1635–1638. https://doi.org/10.1093/bioinformatics/bti236.

Lee, J.-S., Lin, C.-J., Lee, W.-C., Teng, H.-Y., Chuang, M.-H., 2022. Production of succinic acid through the fermentation of *Actinobacillus succinogenes* on the hydrolysate of Napier grass. Biotechnol. Biofuels Bioprod. 15, 9. https://doi.org/10.1186/s13068-022-02106-0.

Li, M.-Y., Liu, H.-Y., Wu, D.-T., Kenaan, A., Geng, F., Li, H.-B., Gunaratne, A., Li, H., Gan, R.-Y., 2022. L-theanine: a unique functional amino acid in tea (*Camellia sinensis* L.) with multiple health benefits and food applications. Front. Nutr. 9, 853846. https://doi.org/10.3389/fnut.2022.853846.

Liu, Q., Bi, H., Wang, K., Zhang, Y., Chen, B., Zhang, H., Wang, M., Fang, Y., 2023. Revealing the mechanisms of enhanced β-farnesene production in *Yarrowia lipolytica* through metabolomics analysis. Int. J. Mol. Sci. 24, 17366. https://doi.org/10.3390/ijms242417366.

Mao, Y., Li, G., Chang, Z., Tao, R., Cui, Z., Wang, Z., Tang, Y.-J., Chen, T., Zhao, X., 2018. Metabolic engineering of *Corynebacterium glutamicum* for efficient production of succinate from lignocellulosic hydrolysate. Biotechnol. Biofuels 11, 95. https://doi.org/10.1186/s13068-018-1094-z.

Mu, W., Zhang, T., Jiang, B., 2015. An overview of biological production of L-theanine. Biotechnol. Adv. 33, 335–342. https://doi.org/10.1016/j.biotechadv.2015.04.004.

Ohtake, T., Pontrelli, S., Laviña, W.A., Liao, J.C., Putri, S.P., Fukusaki, E., 2017. Metabolomics-driven approach to solving a CoA imbalance for improved 1-butanol production in *Escherichia coli*. Metab. Eng. 41, 135–143. https://doi.org/10.1016/j.ymben.2017.04.003.

Polen, T., Schluesener, D., Poetsch, A., Bott, M., Wendisch, V.F., 2007. Characterization of citrate utilization in *Corynebacterium glutamicum* by transcriptome and proteome analysis. FEMS Microbiol. Lett. 273, 109–119. https://doi.org/10.1111/j.1574-6968.2007.00793.x.

Regueira-Marcos, L., García-Depraect, O., Muñoz, R., 2023. Elucidating the role of pH and total solids content in the co-production of biohydrogen and carboxylic acids from food waste via lactate-driven dark fermentation. Fuel 338, 127238. https://doi.org/10.1016/j.fuel.2022.127238.

Sasaki, Y., Eng, T., Herbert, R.A., Trinh, J., Chen, Y., Rodriguez, A., Gladden, J., Simmons, B.A., Petzold, C.J., Mukhopadhyay, A., 2019. Engineering *Corynebacterium glutamicum* to produce the biogasoline isopentenol from plant biomass hydrolysates. Biotechnol. Biofuels 12, 41. https://doi.org/10.1186/s13068-019-1381-3.

Schulz, S., Molitor, B., Angenent, L.T., 2023. Acetate augmentation boosts the ethanol production rate and specificity by Clostridium ljungdahlii during gas fermentation with pure carbon monoxide. Bioresour. Technol. 369, 128387. https://doi.org/10.1016/j.biortech.2022.128387.

Sharkey, M.A., Maher, M.A., Guyonvarch, A., Engel, P.C., 2011. Kinetic characterisation of recombinant *Corynebacterium glutamicum* NAD^+-dependent LDH over-expressed in *E. coli* and its rescue of an lldD2 phenotype in *C. glutamicum*: the issue of reversibility re-examined. Arch. Microbiol. 193, 731–740. https://doi.org/10.1007/s00203-011-0711-z.

Sohn, Y.J., Kang, M., Baritugo, K.-A., Son, J., Kang, K.H., Ryu, M.-H., Lee, S., Sohn, M., Jung, Y.J., Park, K., 2021. Fermentative high-level production of 5-hydroxyvaleric acid by metabolically engineered *Corynebacterium glutamicum*. ACS Sustain. Chem. Eng. 9, 2523–2533. https://doi.org/10.1021/acssuschemeng.0c08546.

Sohn, Y.J., Kang, M., Ryu, M.-H., Lee, S., Kang, K.H., Hong, Y., Song, B.K., Park, K., Park, S.J., Joo, J.C., 2022. Development of a bio-chemical route to C5 plasticizer synthesis using glutaric acid produced by metabolically engineered *Corynebacterium glutamicum*. Green Chem. 24, 1590–1602. https://doi.org/10.1039/D1GC02686K.

Sohn, Y.J., Kim, H.T., Kang, M., Son, J., Park, K., Jeong, K.J., Lee, S.Y., Joo, J.C., Park, S.J., 2025. Metabolic engineering of *Corynebacterium glutamicum* for highly selective production of 5-hydroxyvaleric acid. Metab. Eng. 90, 33–42. https://doi.org/10.1016/j.ymben.2025.03.002.

Son, J., Baritugo, K.-A., Sohn, Y.J., Kang, K.H., Kim, H.T., Joo, J.C., Park, S.J., 2022. Production of γ-aminobutyrate (GABA) in recombinant *Corynebacterium glutamicum* by expression of glutamate decarboxylase active at neutral pH. ACS Omega 7, 29106–29115. https://doi.org/10.1021/acsomega.2c02971.

Stanciugelu, S.I., Patrascu, J.M., Patrascu Jr, J.M., Socaciu, C., Socaciu, A.I., Nitusca, D., Marian, C., 2024. Lipidomic signature of plasma and synovial fluid in patients with osteoarthritis: putative biomarkers determined by UHPLC-QTOF-ESI+ MS. Diagnostics 14, 1834. https://doi.org/10.3390/diagnostics14161834.

Stein, S.E., 1999. An integrated method for spectrum extraction and compound identification from gas chromatography/mass spectrometry data. ASMS 10, 770–781. https://doi.org/10.1016/S1044-0305(99)00047-1.

Styczynski, M.P., Moxley, J.F., Tong, L.V., Walther, J.L., Jensen, K.L., Stephanopoulos, G. N., 2007. Systematic identification of conserved metabolites in GC/MS data for metabolomics and biomarker discovery. Anal. Chem. 79, 966–973. https://doi.org/10.1021/ac0614846.

Tian, Z., Liu, L., Wu, L., Yang, Z., Zhang, Y., Du, L., Zhang, D., 2024. Enhancement of vitamin B6 production driven by omics analysis combined with fermentation optimization. Microb. Cell Fact. 23, 137. https://doi.org/10.1186/s12934-024-02405-1.

van Dijk, M., Mierke, F., Nygård, Y., Olsson, L., 2020. Nutrient-supplemented propagation of *Saccharomyces cerevisiae* improves its lignocellulose fermentation ability. AMB Express 10, 157. https://doi.org/10.1186/s13568-020-01070-y.

Wan, S., Liu, X., Sun, W., Lv, B., Li, C., 2023. Current advances for omics-guided process optimization of microbial manufacturing. Bioresour. Bioprocess. 10, 30. https://doi.org/10.1186/s40643-023-00647-2.

Wang, N., Chen, X.-L., Gao, C., Peng, M., Wang, P., Zhang, N., Li, F., Yang, G.-P., Shen, Q.-T., Li, S., 2021. Crystal structures of γ-glutamylmethylamide synthetase provide insight into bacterial metabolism of oceanic monomethylamine. J. Biol. Chem. 296, 100081. https://doi.org/10.1074/jbc.RA120.015952.

Wehrs, M., Tanjore, D., Eng, T., Lievense, J., Pray, T.R., Mukhopadhyay, A., 2019. Engineering robust production microbes for large-scale cultivation. Trends Microbiol. 27, 524–537. https://doi.org/10.1016/j.tim.2019.01.006.

Xiao, S., Qian, R., Hu, S., Fu, Z., Bai, T., Wang, W., Cheng, J., Zhang, J., 2023. Advances in the production of Theanine by Plants and Microorganisms. Fermentation 9, 543. https://doi.org/10.3390/fermentation9060543.

Yamamoto, S., Wakayama, M., Tachiki, T., 2008. Cloning and expression of *Methylovorus mays* no. 9 gene encoding γ-glutamylmethylamide synthetase: an enzyme usable in theanine formation by coupling with the alcoholic fermentation system of baker's yeast. Biosci. Biotech. Bioch. 72, 101–109. https://doi.org/10.1271/bbb.70462.

Yang, P., Liu, W., Cheng, X., Wang, J., Wang, Q., Qi, Q., 2016. A new strategy for production of 5-aminolevulinic acid in recombinant *Corynebacterium glutamicum* with high yield. Appl. Environ. Microbiol. 82, 2709–2717. https://doi.org/10.1128/AEM.00224-16.

Yang, Q., Cai, D., Chen, W., Chen, H., Luo, W., 2022. Combined metabolic analyses for the biosynthesis pathway of l-threonine in *Escherichia coli*. Front. Bioeng. Biotechnol. 10, 1010931. https://doi.org/10.3389/fbioe.2022.1010931.

Yang, T., Zhang, D., Cai, M., Zhang, H., Pan, X., You, J., Zhang, X., Xu, M., Rao, Z., 2024. Combining protein and metabolic engineering strategies for high-level production of

L-theanine in *Corynebacterium glutamicum*. Bioresour. Technol. 394, 130200. https://doi.org/10.1016/j.biortech.2023.130200.
Zhong, Z., Ma, Z., Cao, Y., Zhang, H., Qi, Y., Wei, L., Jiang, J., Xu, N., Liu, J., 2025. Metabolic engineering of *Corynebacterium glutamicum* for efficient L-homoserine production from lignocellulose-derived sugars. ACS Sustain. Chem. Eng. 13, 3441–3451. https://doi.org/10.1021/acssuschemeng.4c07838.
Zhou, S., Zhang, D., Xu, M., Zhang, X., Yang, T., Rao, Z., 2025. Metabolic engineering of *Escherichia coli* for de novo synthesis of L-theanine. Chin. J. Biotechnol. 41, 3459–3472. https://doi.org/10.13345/j.cjb.250103.

Glossary

5-HV: 5-hydroxyvaleric acid
ATP: adenosine triphosphate
EcGCS: L-glutamate–L-cysteine ligase from *Escherichia coli*
GC–MS: gas chromatography–mass spectrometry
GMAS: γ-glutamylmethylamide synthetase
MSEA: metabolite set enrichment analysis
NADH: nicotinamide adenine dinucleotide
NADPH: nicotinamide adenine dinucleotide phosphate
OPLS-DA: orthogonal partial least squares discriminant analysis
PCR: polymerase chain reaction
PLS-DA: partial least squares discriminant analysis
SSB: sweet sorghum bagasse
TCA: tricarboxylic acid
THE-1 to THE-6: theanine-producing recombinant strains
VIP: variable importance in projection
XGM: mixed sugars (xylose, galactose, and mannose)
LC-MS/MS: liquid chromatography-tandem mass spectrometry